NUREG/CR-4625
SAND86-1102

# Postirradiation Examination of the DC Melt Dynamics Experiments

Prepared by C.P. Fryer, J.T. Hitchcock

Sandia National Laboratories

Prepared for
U.S. Nuclear Regulatory
Commission

NOTICE

Availability of Reference Materials Cited in NRC Publications

Most documents cited in NRC publications will be available from one of the following sources:

1. The NRC Public Document Room, 1717 H Street, N.W. Washington, DC 20555
2. The Superintendent of Documents, U.S. Government Printing Office, Post Office Box 37082, Washington, DC 20013-7082
3. The National Technical Information Service, Springfield, VA 22161

Although the listing that follows represents the majority of documents cited in NRC publications, it is not intended to be exhaustive.

Referenced documents available for inspection and copying for a fee from the NRC Public Document Room include NRC correspondence and internal NRC memoranda; NRC Office of Inspection and Enforcement bulletins, circulars, information notices, inspection and investigation notices; Licensee Event Reports; vendor reports and correspondence; Commission papers; and applicant and licensee documents and correspondence.

The following documents in the NUREG series are available for purchase from the GPO Sales Program: formal NRC staff and contractor reports, NRC-sponsored conference proceedings, and NRC booklets and brochures. Also available are Regulatory Guides, NRC regulations in the *Code of Federal Regulations*, and *Nuclear Regulatory Commission Issuances*.

Documents available from the National Technical Information Service include NUREG series reports and technical reports prepared by other federal agencies and reports prepared by the Atomic Energy Commission, forerunner agency to the Nuclear Regulatory Commission.

Documents available from public and special technical libraries include all open literature items, such as books, journal and periodical articles, and transactions. *Federal Register* notices, federal and state legislation, and congressional reports can usually be obtained from these libraries.

Documents such as theses, dissertations, foreign reports and translations, and non-NRC conference proceedings are available for purchase from the organization sponsoring the publication cited.

Single copies of NRC draft reports are available free, to the extent of supply, upon written request to the Division of Information Support Services, Distribution Section, U.S. Nuclear Regulatory Commission, Washington, DC 20555.

Copies of industry codes and standards used in a substantive manner in the NRC regulatory process are maintained at the NRC Library, 7920 Norfolk Avenue, Bethesda, Maryland, and are available there for reference use by the public. Codes and standards are usually copyrighted and may be purchased from the originating organization or, if they are American National Standards, from the American National Standards Institute, 1430 Broadway, New York, NY 10018.

NUREG/CR-4625
SAND86-1102
R7

# THE POSTIRRADIATION EXAMINATION OF THE DC MELT DYNAMICS EXPERIMENTS

C. P. Fryer
J. T. Hitchcock

July 1988

ndia National Laboratories
Albuquerque, NM 87185
Operated by
Sandia Corporation
for the
U.S. Department of Energy

Prepared for
Division of Reactor Accident Analysis
Office of Nuclear Regulatory Research
U.S. Nuclear Regulatory Commission
Washington, DC 20555
Under Memorandum of Understanding DOE 40-550-75
NRC FIN NO. A1181

Abstract

The Dry Capsule experiment series investigates the coolability of dry fast reactor core debris through nuclear heating of actual reactor materials in order to obtain the thermal properties of dry debris, the nature of the transition from a debris bed to a molten pool, and the thermal and kinetic behavior of molten pools. The purpose is to develop a data base in support of model development. The work is jointly sponsored by the US Nuclear Regulatory Commission (USNRC), the Power Reactor and Nuclear Fuel Development Corporation (PNC, Japan), and Joint Research Centre, Ispra (EURATOM).

This report provides a brief description of the two experiments in the Dry Capsule series and presents the results of the postirradiation examination. These tests investigated dry debris beds (~2 kg) composed of pure $UO_2$ and mixed $UO_2$ and stainless steel. The beds were taken into melt to observe the growth of a molten pool in the $UO_2$ bed and the agglomeration and migration of steel in a composite bed. The peak measured temperature in the $UO_2$ bed was above 3100°C. Approximately 50 percent of the urania formed a molten pool. Surrounding the molten pool and an overlying void was a high density urania crust. Lenticular pore formation and migration caused by urania vapor transport in the strong thermal gradient were seen in the urania crust. In the mixed $UO_2$ and steel bed, the peak measured temperature was 2600°C. All of the steel had been molten. Steel and urania migration were observed; both were thought to be caused by vapor transport mechanisms.

CONTENTS

## List of Figures

List of Tables

1. INTRODUCTION

The Dry Debris Coolability Program at Sandia National Laboratories investigates the coolability of particle beds that may form following a severe accident involving core disassembly in a Liquid Metal Fast Breeder Reactor (LMFBR). This debris is capable of generating significant power through the decay of fission products. If debris beds are flooded, initial cooling is provided through conduction, convection, and boiling of the coolant. If the decay heat power is sufficiently high, a bed may dry out leaving debris cooled primarily by conduction and radiation. With insufficient cooling, the debris will proceed into melt and may threaten the vessel. Reactor safety analyses typically assume that debris dryout represents the coolability limit. However, results from debris bed studies at Sandia indicate that dryout may not represent the upper coolable configuration. Stable conditions which pose no threat to reactor structures may occur with portions of debris beds dried out. In order to define the ultimate coolability limits, it is necessary to determine the thermal characteristics of dry core debris and the processes of molten pool formation. The Dry Capsule (DC) experiment series investigates the coolability of dry fast reactor core debris through nuclear heating of actual reactor materials in order to obtain the thermal properties of dry debris, the nature of the transition from a debris bed to a molten pool, and the thermal and kinetic behavior of molten pools. The purpose is to develop a data base in support of model development. The work is jointly sponsored by the US Nuclear Regulatory Commission (USNRC), the Power Reactor and Nuclear Fuel Development Corporation (PNC, Japan), and Joint Research Centre, Ispra (EURATOM).

The Dry Capsule experiments investigated dry debris beds composed of pure $UO_2$ (DC-1) and mixed $UO_2$ and stainless steel (DC-2). The experiments were performed in-pile in the Annular Core Research Reactor (ACRR) to obtain prototypic internal heating. The capsules were cooled on top and bottom by a closed loop helium system which allowed steady-state operation. Sides were insulated to reduce radial heat losses. The experiments were carried out in two parts. First, the heat transfer characteristics of dry porous particulate beds were studied. Several steady-state conditions were established at various temperatures below melt to obtain data on the bed thermal conductivity. Low temperature data were used for comparison with out-of-pile measurements. High-temperature data provided unique information on the total effective conductivity in the range where radiative heat transfer dominated. The $UO_2$/steel bed provided data on the effect of multiple solid components. Second, the beds were taken into melt to observe the melt progression in a $UO_2$ bed and the agglomeration and migration of steel in a composite bed.

The Dry Capsule program is an extension of the sodium coolability work at Sandia. In complementary D-series experiments, dryout criteria were investigated using full-height debris beds with overlying sodium pools. However, these experiments were limited to submelting temperatures to avoid the safety considerations of possible molten fuel/sodium interaction upon liquid reentry. The later stages of the postulated accidents were investigated separately in the Dry Capsule program by simulating only the dry portion of the debris beds and using argon gas to simulate sodium vapor. The results from the DC experiments are also applicable to dried out regions which may exist in light water reactor degraded cores.

This report provides a brief description of the two experiments in the Dry Capsule series and presents the results of the postirradiation examination of the two beds. This report complements the experiment report,[1] which is a full description of the experiment and includes all of the thermal data.

## 2. EXPERIMENT OBJECTIVES

The DC tests are phenomenological experiments and are directed toward support of model development and verification. The purpose is twofold: (1) to develop a data base on the thermal characteristics and behavior of dry reactor debris under extreme temperatures and prototypic thermal gradients and (2) to understand the phenomena associated with melt of structural and fuel materials. As such, pure materials were chosen along with analyzable geometry.

The objectives of DC-1 were to investigate the thermal characteristics of an internally-heated $UO_2$ debris bed from 1000°C to melt and to understand the phenomenology and thermal characteristics of a molten $UO_2$ pool. Bed and capsule temperature distributions were measured at several steady-state conditions during the test and phenomenological data were obtained by microscopic examination of the bed upon experiment disassembly. The temperature data is used to obtain high-temperature heat transfer rates in pure $UO_2$ debris and the bed heat partition, that is, the upward, downward, and radial heat flux. Microscopic examination of the bed provides information on the process of melting; the mechanism for crust formation is of specific interest.

The DC-2 test investigated the behavior of a composite bed composed of 75 wt% $UO_2$ and 25 wt% stainless steel. Temperature distributions were measured at several steady-state conditions to provide the thermal characteristics of the bed and to verify models of the effective conductivity of porous beds with multiple solid components. Molten steel migration and agglomeration behavior in a large thermal gradient were studied posttest by microscopic examination of the bed.

## 3. CAPSULE DESIGN

The experiment capsule used in both DC-1 and DC-2 is shown in Figure 1. Radiological containment was provided by two separate stainless steel vessels. The bottom and sidewall of both vessels were made of thick steel to act as a core catcher and heat sink in case of crucible failure or loss of cooling. A closed-loop helium system provided active cooling and permitted steady-state operation. During the tests, the bed was centered at the midplane of the ACRR core.

The debris bed was contained in a single piece hot-spun tungsten crucible. It was supported above the primary vessel lid by tantalum rods and was spring loaded against the bottom of the primary vessel. The bed was side insulated, first by an 8-mm-thick $ThO_2$ liner inside of the crucible and then by a low-density $ZrO_2$ board (86 percent porous) between the crucible and containment sidewalls. In DC-2 the 1.4-mm gap between the $ThO_2$ liner and the crucible was filled with $ThO_2$ powder to provide a large surface area barrier to molten steel in case the liner fractured and steel moved toward the crucible.

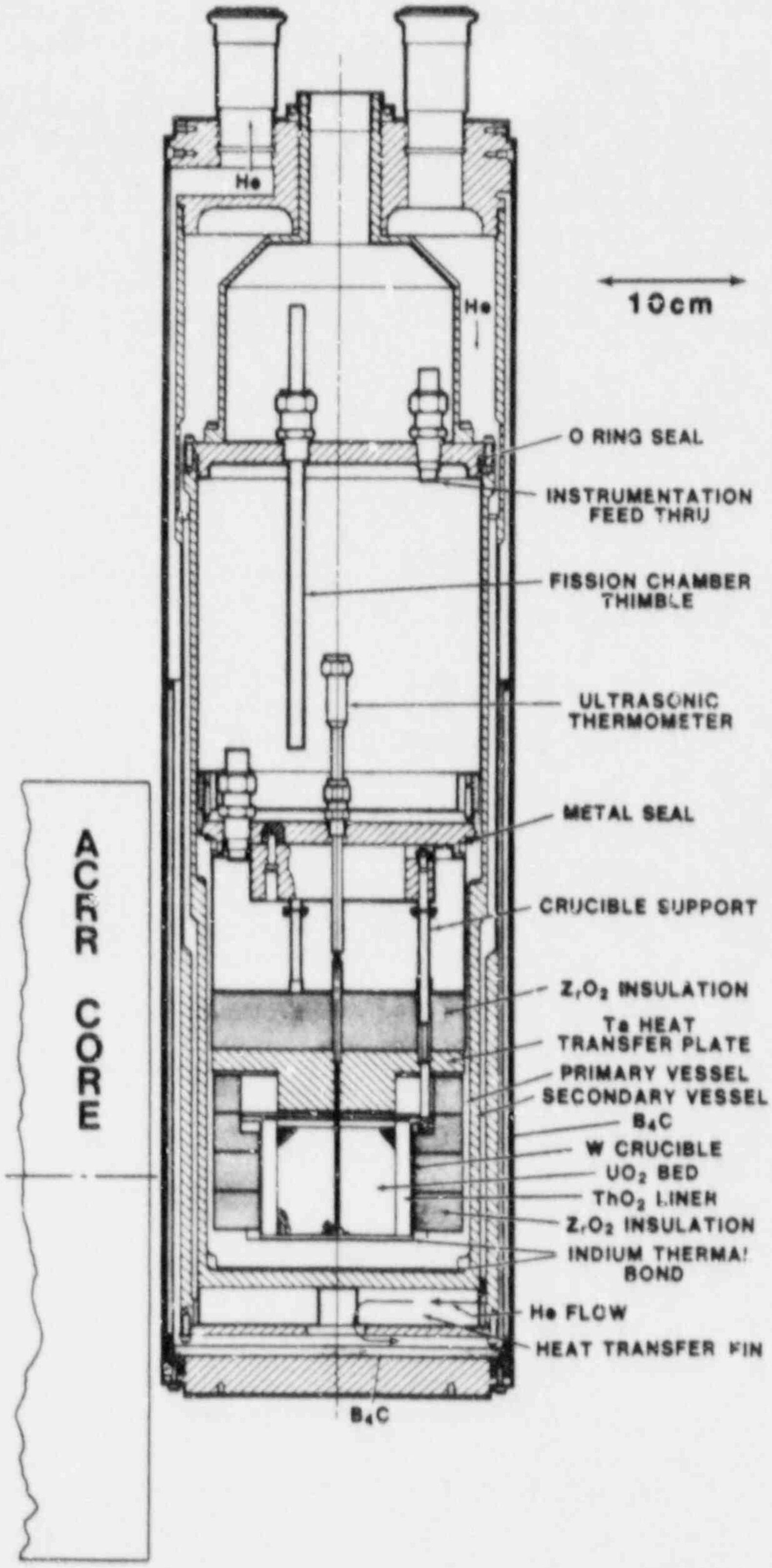


Figure 1. Dry Capsule Test Configuration

The bed in each test was cooled at top and bottom. The top was cooled by radiation to a tantalum plate which shunted the heat to the containment sidewalls. The bottom surface of the tantalum was grit blasted and slightly oxidized to increase the emissivity. The bottom was cooled by conduction through the primary containment to fins attached to the bottom of the secondary vessel. Indium (melting point 150°C and boiling point 2000°C) was used to couple the crucible to the primary containment and the primary to the secondary containment for enhanced heat transfer. Heat was removed from the secondary containment vessel by helium flowing down the sidewalls and across the bottom fins. The helium then flowed up an outer annular passage and out of the package to a heat exchanger. The resulting temperature distribution of the bed was not axially symmetric or completely one-dimensional because of the lower effectiveness of the radiative cooling and radial heat loss. At peak power conditions in DC-1, the temperature of the center of the bed was 3100°C; the bottom, 700°C; the top, 1700°C; and the periphery, 2500°C.

The $B_4C$ neutron filters used in the capsule were to harden the neutron spectrum and flatten the bed power deposition profile. An annular filter of 3-mm-thick $B_4C$ powder was located adjacent to the outer wall of the helium chamber. A pressed $B_4C$ disc was also positioned below the bed. The top of the bed was shielded by the tantalum heat transfer plate. The resulting peak-to-average power ratio in the bed was calculated to be 1.18.

The primary vessel was backfilled with argon gas at $3.4 \times 10^4$ Pa(abs.). The thermal properties of argon closely approximate those of sodium vapor. The secondary vessel was backfilled with $6.8 \times 10^4$ Pa(abs.) of helium to enhance the heat transfer between vessels.

## 4. BED DESCRIPTION

The fuel used in the DC-1 and DC-2 debris beds was composed of a homogeneous mixture of fully enriched $UO_2$ particulate ranging in size from 0.090 to 1.0 mm. The particles were prepared by Los Alamos National Laboratory by reduction of $UO_3$ in flowing hydrogen for one hour at 650°C followed by sintering for one hour in flowing helium and water vapor to obtain a ceramic $UO_2$, stable in air. The $UO_2$ thus prepared was then pressed, crushed, sieve sized, and fired at 1800°C for 24 h in hydrogen. The fired particles were further crushed and sieve sized to obtain the final particle distribution. Additionally, the $UO_2$ was baked out at 250 to 300°C for 24 h under vacuum following loading into the experiment.

In DC-1, the bed was composed of 2.138 kg of $UO_2$, 70 mm high and 80 mm in diameter. The effective particle diameter, calculated by the Fair-Hatch formula,[2] was 240 $\mu m$. The bed was formed by carefully spooning a well-mixed batch of $UO_2$ into the crucible. The final bed height was estimated to have an uncertainty of about 1 mm. The measured density of the $UO_2$ particulate itself was 93 percent of theoretical, and the resulting bed density was 6000 $kg/m^3$. The open porosity (not including porosity within particulate) in the bed was 41.2 percent. It should be noted that these were as-built dimensions and densities. However, since vibration and jolting occurred during subsequent assembly, testing, and loading of the experiment, some settling did occur. Similar beds, subjected to an arbitrary amount of tapping to approximate the experiment handling, increased in density about 100 to 200 $kg/m^3$. Each 100 $kg/m^3$ increase in density corresponds to a 1 percent decrease in porosity. The detailed specifications of the DC-1 bed are listed in Table 1.

Table 1
Bed Description for DC-1 and DC-2

| | DC-1 | DC-2 |
|---|---|---|
| Total $UO_2$ Mass | 2.1383 kg | 1.5352 kg |
| Total Steel Mass | -- | 0.5105 kg |
| Total Bed Mass | 2.1383 kg | 2.0457 kg |
| Bed Diameter | 80.77 mm | 80.39 mm |
| Bed Height | 70 ± 1 mm | 70 ± 1 mm |
| Gross Bed Volume | 358 $cm^3$ | 355 $cm^3$ |
| Bed Instr. Volume | 2.4 $cm^3$ | 5.6 $cm^3$ |
| Net Bed Volume | 356 $cm^3$ | 350 $cm^3$ |
| Bed Density | 6006 $kg/m^3$ | 5845 $kg/m^3$ |
| Avg. $UO_2$ Particle Density ($TD=10.97\ g/cm^3$) | 93.0% TD | 93.8% TD |
| Bed Open Porosity | 41.2% | 39.0% |
| Eff. $UO_2$ Particle Diameter | 240 $\mu m$ | 240 $\mu m$ |
| Eff. Steel Particle Diameter | -- | 438 $\mu m$ |
| Eff. Bed Particle Diameter | 240 $\mu m$ | 270 $\mu m$ |
| $UO_2$ Stoichiometry (XRD) | 2.0004±0.0016 to 2.0022±0.0006 | same |

The bed in DC-2 had the same nominal dimensions as in DC-1. It consisted of a homogeneous mixture of 1.535 kg of fully enriched $UO_2$ and 0.511 kg of 316L stainless steel particulate. The average $UO_2$ particle density was slightly higher at 93.8 percent of theoretical density, and the final bed density was 5850 $kg/m^3$. The resulting bed open porosity was 39 percent. Stainless steel fragmented by inert gas to minimize the amount of dissolved oxygen was used in the bed. The resulting spherical particles were etched to remove any surface oxidation. Chemical analysis indicated that the oxygen content in the steel was 110 ppm and was uniform for all particle sizes. The size distribution of the $UO_2$ was identical to that used in DC-1. The prototypic size distribution for the steel was a factor of 2 larger than the $UO_2$; however, the maximum size available from the fragmentation method was 1 mm. Calculation of the effective particle sizes yields 240 $\mu m$ for the $UO_2$, 438 $\mu m$ for the steel, and 270 $\mu m$ for the composite bed. The detailed specifications of the DC-2 bed are listed in Tables 1 and 2.

Table 2
Composition of Steel Particulate in DC-2

Type: 316L

Tested Components

| | |
|---|---|
| Oxygen | 0.011% |
| Nitrogen | 0.107% |
| Carbon | 0.022% |
| Silicon | 0.65% |
| Manganese | 0.72% |
| Phosphorus | 0.023% |
| Sulfur | 0.007% |
| Chromium | 16.9% |
| Nickel | 11.2% |
| Molybdenum | 2.08% |
| Iron | Balance |

## 5. INSTRUMENTATION

Instrumentation for these experiments consisted of four ultrasonic thermometers (UT)[3] and five W/Re thermocouples. The ultrasonic thermometers consisted of a tungsten sensor inside of a $ThO_2$ sheath. In DC-1, an outer protective tungsten sheath was added to isolate the $ThO_2$ from molten $UO_2$. A depleted $UO_2$ thimble was placed between this tungsten sheath and the crucible to reduce shunting of heat to the crucible. In the ultrasonic thermometer, an average temperature across a sensor interval is obtained. Each sensor has five intervals of 10 mm, giving five temperature measurements per UT. The ultrasonic thermometers were placed radially at 0, 20, 30, and 40 mm from the bed centerline. The axial measurement zone extended from 25 to 75 mm from the bottom of the bed in DC-1 and from 20 to 70 mm in DC-2.

The bed thermocouples, custom manufactured by Hanford Engineering Development Laboratory, had a tungsten sheath, solid $HfO_2$ insulation, and W-5% Re/W-26% Re thermoelement wires. In DC-2, an outer $ThO_2$ sheath was added to protect the tungsten sheath from molten steel in the bed. Prior to the experiments, prototypical thermocouples were performance tested to 2400°C for 4 h.

Several things should be noted when using data from the bed instrumentation. First, the ultrasonic thermometers measure an average temperature over a 10-mm interval. Second, any instrumentation with a tungsten sheath in a large thermal gradient will locally perturb the bed temperature. Hence, while the temperature measurement of the instrumentation may be accurate, proper interpretation of the temperature distribution in the bed may require three-dimensional analyses.

## 6. EXPERIMENT PROCEDURES

The experimental procedures for DC-1 and DC-2 were sufficiently similar that both can be discussed together with the differences being highlighted. The procedures for each test were formulated to meet two main objectives. The first objective was to attain steady-state temperature distributions at various bed power levels in order to determine the effective thermal conductivity of the debris. The second objective was to melt the $UO_2$ (DC-1) or the steel (DC-2), contain the melt, and obtain data on the heat transfer and physical behavior of the molten material.

Both tests involved first attaining three steady-state conditions at different bed powers before any melting occurred. The entire package was allowed to equilibrate for at least an hour in order to attain a true steady-state condition. This procedure was repeated for each of the steady-state conditions. In DC-1 the peak measured temperatures for the three steps were 975°, 1700°, and 2230°C. For DC-2, the peak measured temperatures for the three steps were 810°, 1080°, and 1340°C.

Following the three steady-state conditions, the reactor power was increased to 2.6 W/g in DC-1 and 2.3 W/g in DC-2 in order to obtain melting in the bed. For DC-1, the goal was to melt approximately half of the $UO_2$. For DC-2, the goal was to attain a maximum bed temperature of 2500°C, at which a significant fraction of the steel would be molten. Once again, the entire package was allowed to equilibrate to attain a steady-state temperature distribution. The beds were held at the maximum temperature approximately 40 min. After the temperature of the molten debris configuration had equilibrated, the reactor power was rapidly reduced to a low value. The temperatures in the debris fell rapidly, and the molten material froze.

After the experiment, the primary containments of DC-1 and DC-2 were filled under vacuum with epoxy mounting medium. From DC-1, a 1-cm-thick slice was cut vertically through the center of the bed with the face of interest through two ultrasonic thermometers and two thermocouples. From DC-2, two 1-cm-thick slices were taken, one from each side of a similar plane. These slices were prepared for macroscopic examination. Small samples were cut from the slices and prepared for optical microscopy. Cutting diagrams are shown in Figure 2.

## 7. POSTTEST STRUCTURAL ANALYSIS

### 7.1 DC-1

DC-1 attained a peak measured temperature of ~3100°C in the center of the bed and ~2500°C at the edge. At peak power, the average radial temperature gradient in the horizontal plane through the center was ~150°C/cm, while vertically above and below the center it was ~400°C/cm and ~700°C/cm, respectively. The posttest bed consisted of a shell of restructured fuel holding a once-molten pool of $UO_2$ (Figure 3). A large void formed above the pool due to the difference in porosity between the initial bed and the molten pool. The final bed height was 66 mm, indicating a compaction of only 4 mm (5 percent). The grain structure of the shell indicates that the hottest zone prior to molten-pool formation was a shallow, but radially large, disc-shaped area centered 42 to 43 mm above the bottom of the bed. This is substantiated by the location of a breach in the instrument sheaths; note that the lateral as well as central sheaths are affected.

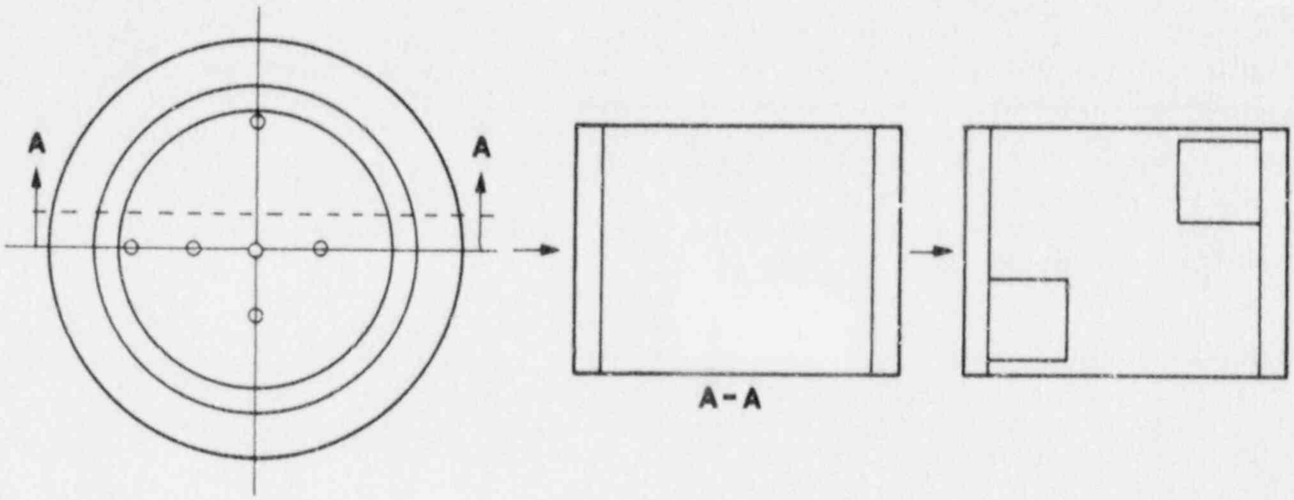


a. DC-1

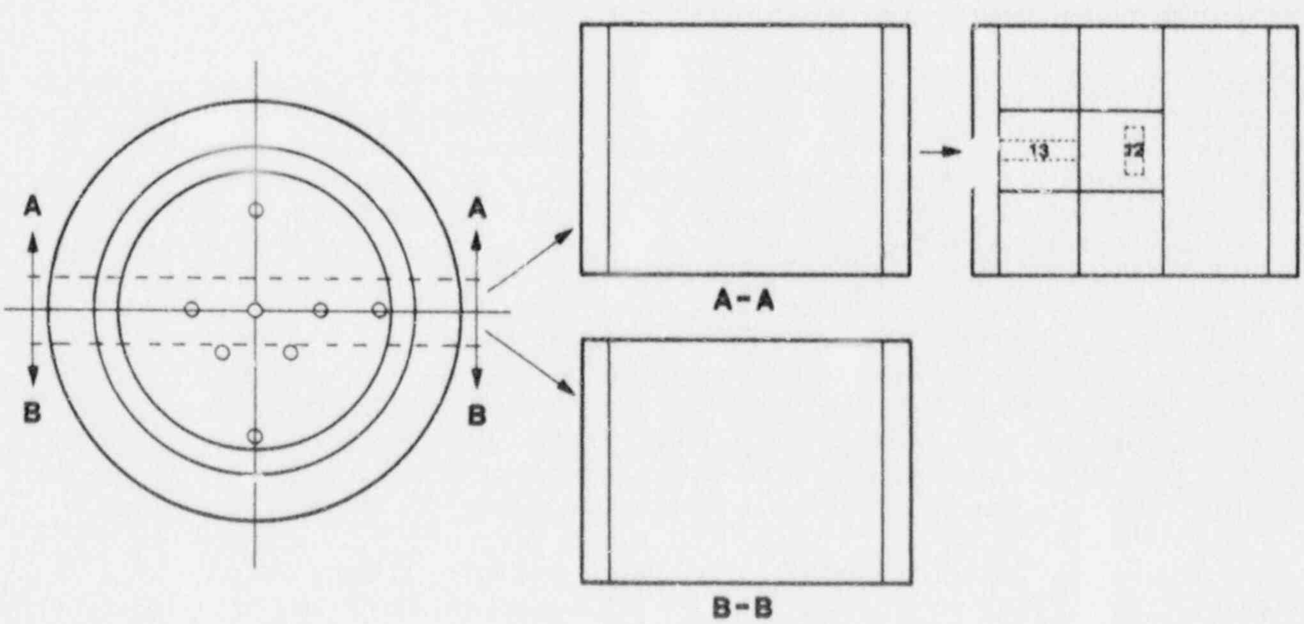


b. DC-2

Figure 2. Posttest Cutting Diagrams, Scale 1:2

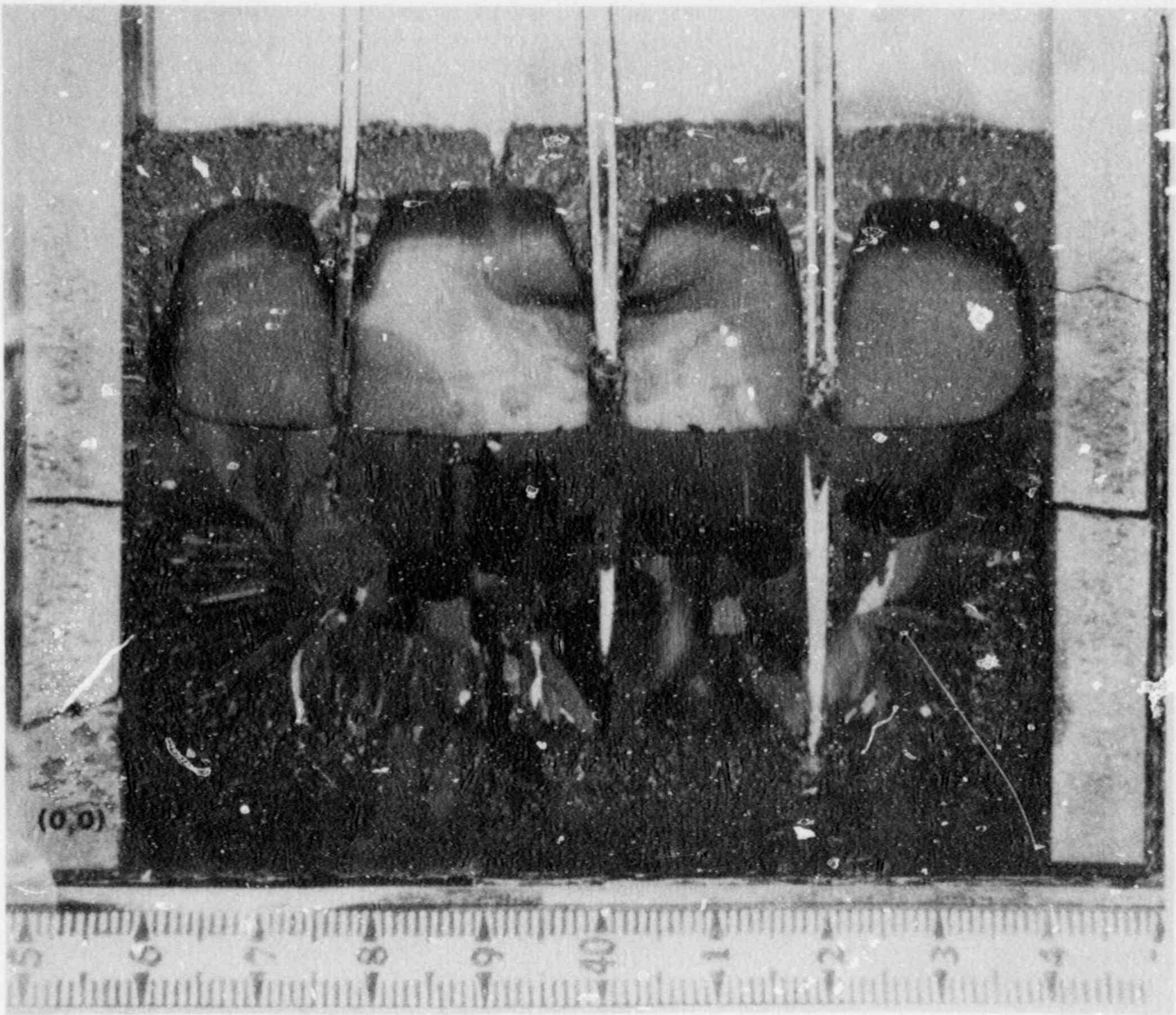

Figure 3. DC-1 Center Plane.
The location of subsequent micrographs is given in mm from the origin as shown.

The columnar grain structure of the solidified pool indicates the direction of heat flow during solidification. The grain structure at the upper edge of the pool shows that the heat removal rate was nearly equal through the side of the bed and from the top. The instrumentation sheaths acted as cold fingers and caused some local temperature disturbances in the bed. The relative heat transfer rate through the bottom of the bed is not as clearly determined due to the presence of the equiaxed zone overlaid by large, linked voids in the center of the solidified pool. The following (based on microstructural evidence) is a possible scenario for the freezing process: The pool begins to freeze with long, columnar grains forming due to the pronounced heat gradient. The heat transfer rate is similar through the top, bottom, and side of the bed. When freezing is ~80 percent complete, the heat removal rate becomes insufficient to support columnar freezing, and the remaining liquid freezes in large (due to the paucity of impurity nucleation sites), equiaxed grains. The large void volume is accounted for by solidification shrinkage, although the morphology is atypical.

For the consideration of the microstructure, the bed was conveniently divided into three parts. These are (1) the outer, unaffected zone, (2) the vapor transport (restructured) zone, and (3) the once-molten zone (Figure 4). The three zones--from lower left to upper right--are seen clearly in Figure 5, which is the lower left hand corner of the polished cross section. The unaffected region, Zone 1, is made up of $UO_2$ particles in which there is no significant change in shape, size, or microstructure as compared to the starting material. The grains are equiaxed, with an average diameter of ~25 $\mu m$. This loose particulate material occupies a small area at the top and bottom of the bed (see Figure 3).

The vapor transport zone, Zone 2, provides an example of the process of material relocation and densification in a steep temperature gradient. In the coldest, or outer, region of the vapor transport zone, small protuberances or fingers formed on the up-gradient (hotter) surfaces of original particles (Figure 6a). These are low porosity single crystals, one to two times as wide as the base grains and several times longer. Those fingers that formed in the hotter regions of the vapor transport zone were larger. The fingers are comprised of one or two crystals of fully dense material, are of a generally angular cross section, and have a leading face, which is perpendicular to the gradient vector. There is some grain growth in the particles of starting material; grains attain an average diameter of ~50 $\mu m$ in the hottest zones. Fingers formed in yet hotter regions of the vapor transport zone contacted the cold ends of hotter particles and formed lenticular pores (Figure 6b), such as are seen in ceramic fuel pellets during initial restructuring.[4] The hottest region of the vapor transport zone consists of dense material through which lenticular pores migrated towards the thermal center of the bed. The pores, which trail voids from their outer edges, moved with their long dimension perpendicular to the temperature gradient (Figure 7). This region is found on the border of the pool and above the large void. In regions in which there was no longer a down-gradient pore source, dense material with a columnar grain structure was attained. Such material is seen near the large void along the crucible walls and the instrument sheaths (Figure 8).

Vapor transport of $UO_2$ molecules from the down-gradient (cold) side of up-gradient (hotter) particles to the up-gradient (hot) side of adjacent down-gradient (colder) particles began as the temperature exceeded approximately 2000°C. (Four previous studies of this phenomenon in oxide fuel rods, cited in Reference 4, have placed the temperature at the equiaxed-columnar region boundary (i.e., the vapor transport boundary) at 1700°, 1800°, 2000°, and 2150°C.) Here, as deposition proceeded, favorably oriented grains grew with respect to other grains to form the "fingers" seen earlier. Less favorably oriented incipient fingers disappeared. The fingers grew parallel to the temperature gradient with one or two flat leading faces. The faces, which are probably low index planes, are not always truly perpendicular to the gradient vector.

Down-gradient vapor transport of material eventually led to the removal of nondensified areas because the vapor deposited material was less porous than the starting material. Most lenticular pore motion occurred through previously densified fuel. There was net movement of fuel out of the hot zone. No conventional sintering of particles was seen.

The molten zone, Zone 3, consists of a pool of once-molten material contained in the restructured material. The microstructure shows large, columnar grains typical of a material solidified in a temperature gradient. There is a small amount of microporosity; the pores, $< 10\ \mu m$ in diameter, are distributed rather evenly between the grain boundaries and the grain interiors (Figure 9a and 9b). The polarized light reveals the grain structure.

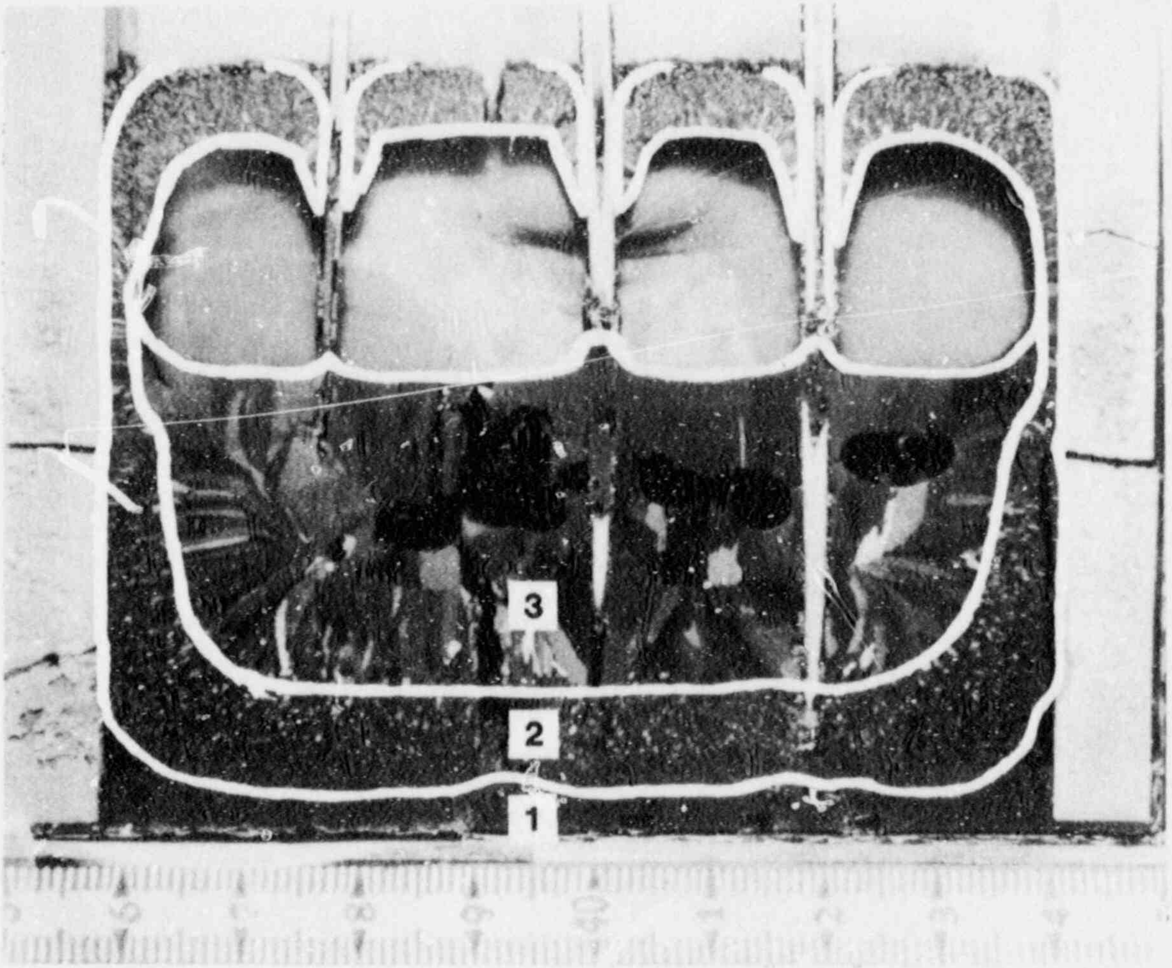


Figure 4. Unaffected (1), Vapor Transport (2), and Molten (3) Zones of DC-1

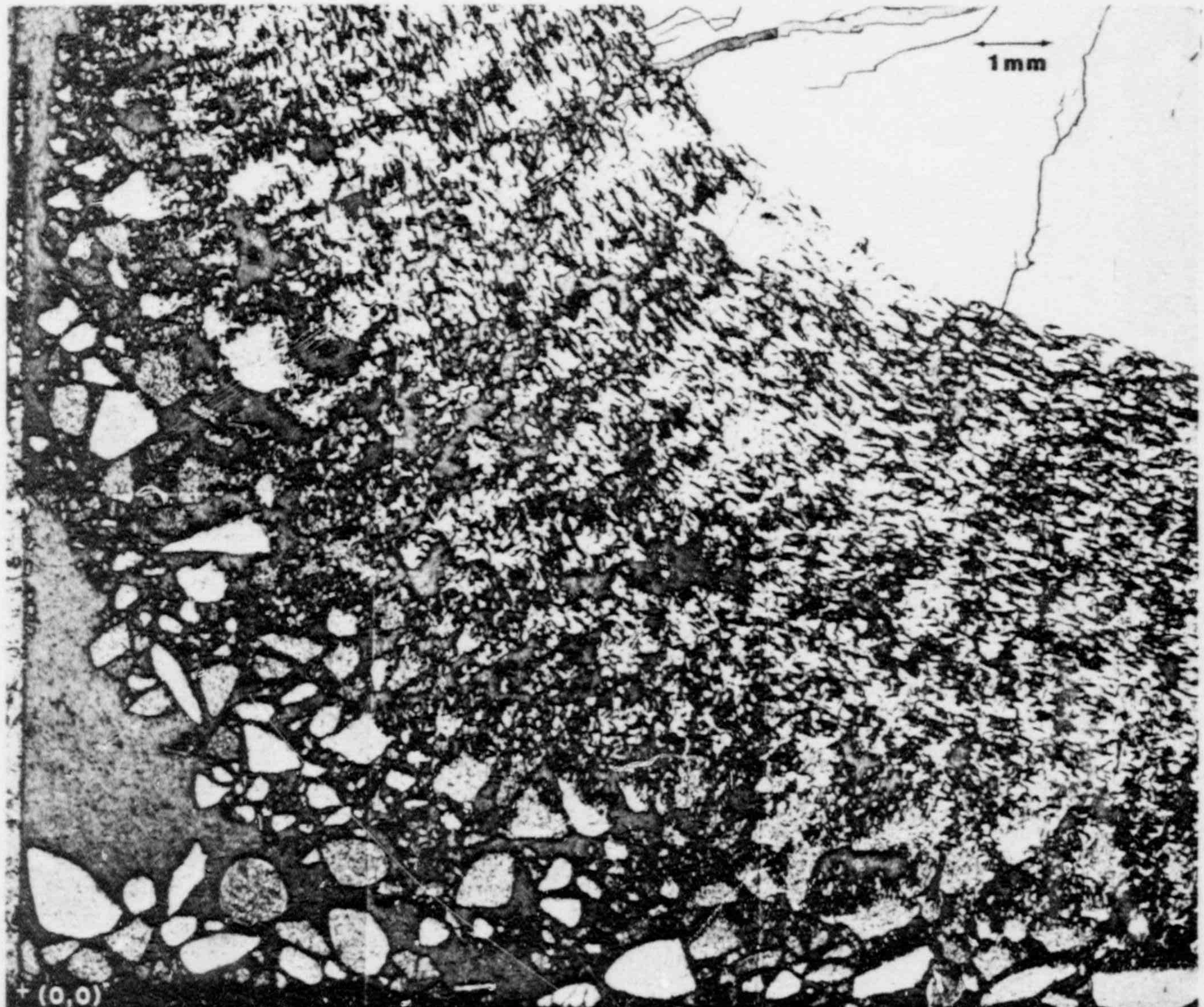


Figure 5 DC-1, Crucible Edge to Molten Zone.
The location of subsequent micrographs is given in mm from the origin as shown.

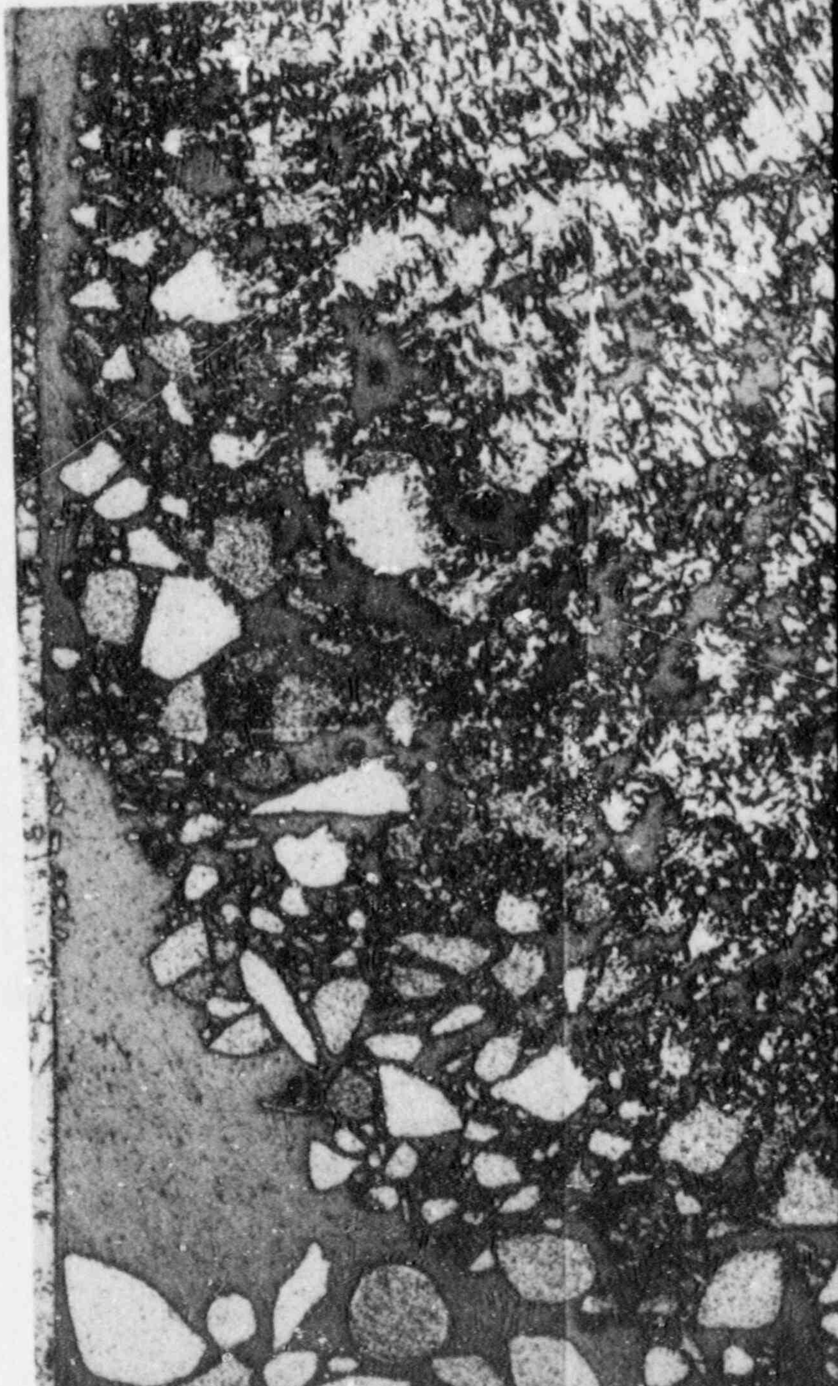


Figure 5 DC-1, Crucible Edge to Molte
The location of subsequent m

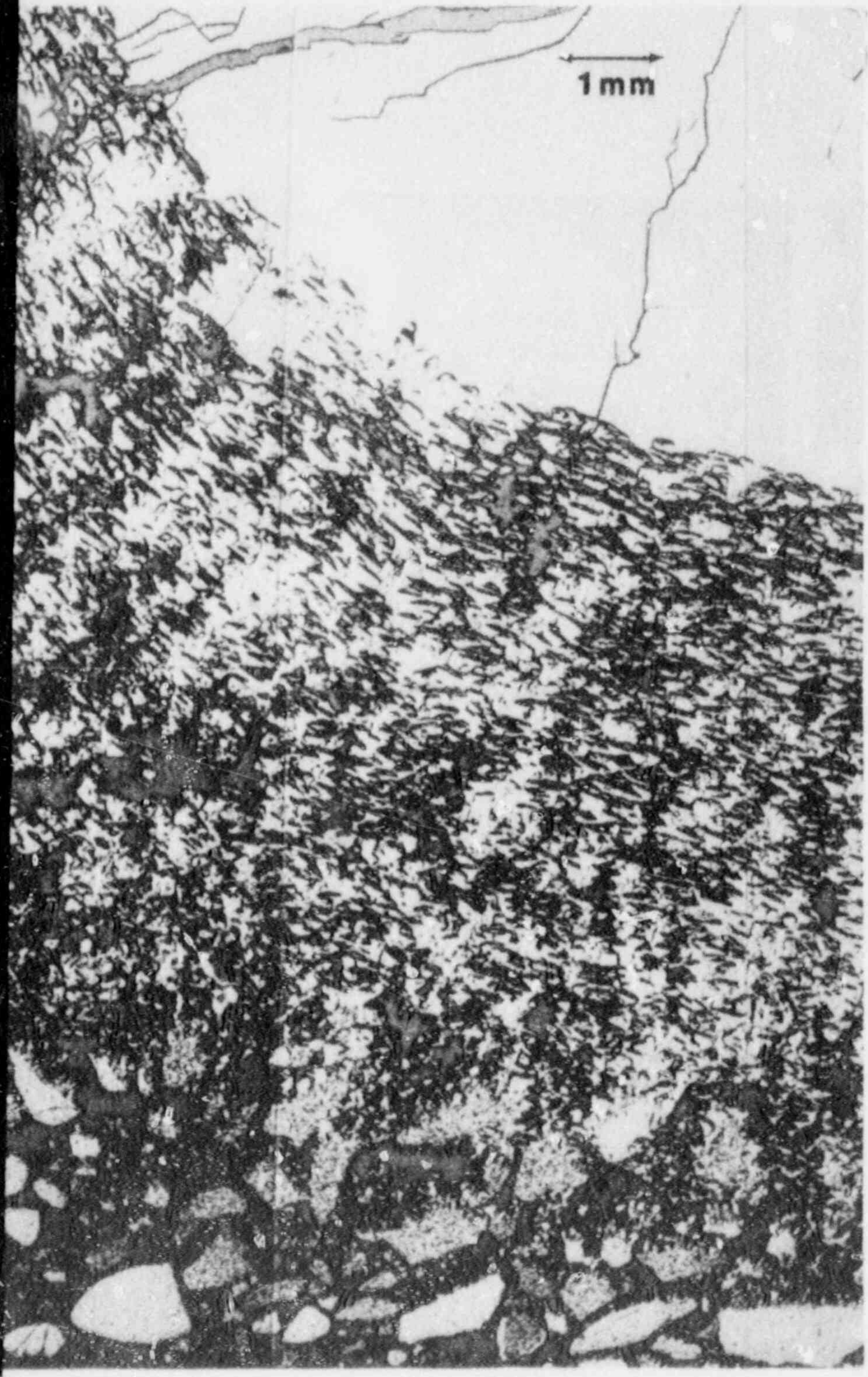




n Zone.
icrographs is given in mm from the origin as shown.

8808120165-01

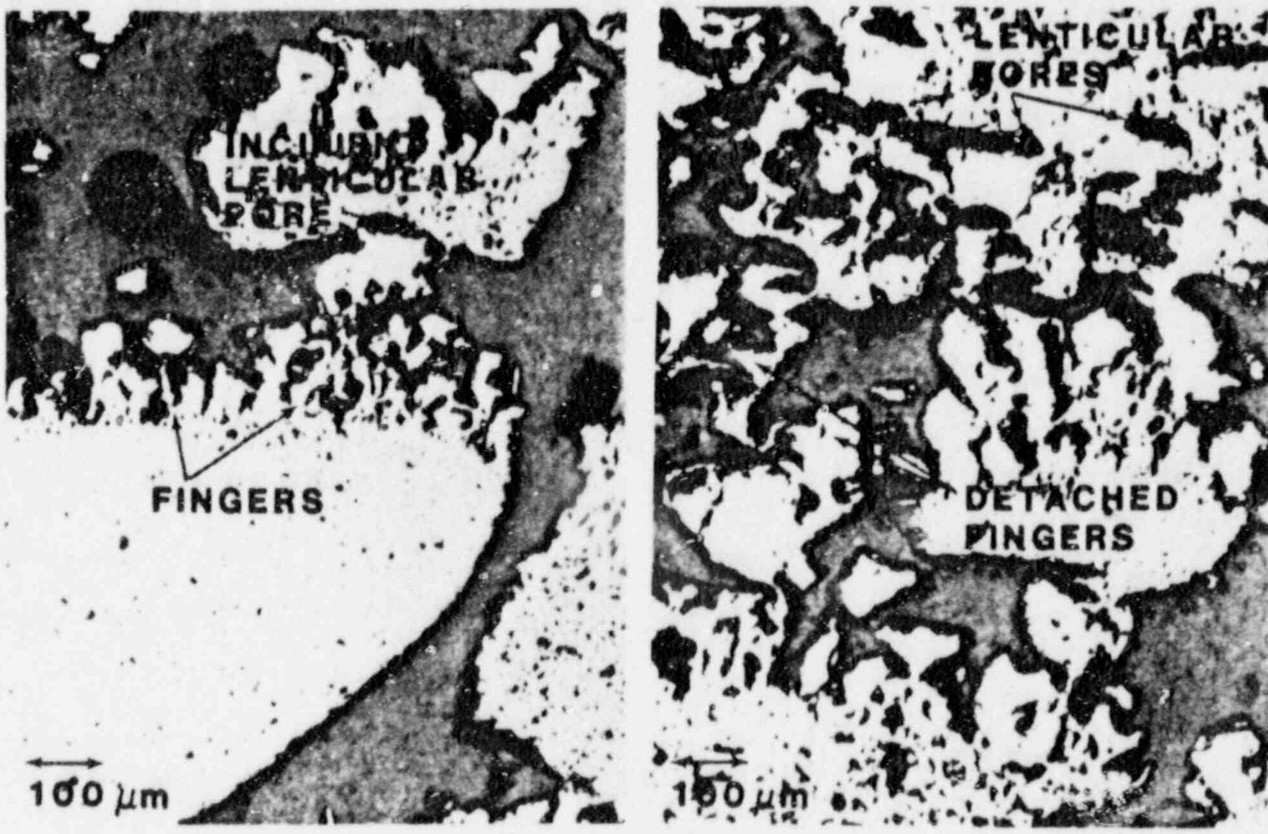


a. Small, densified fingers on large, porous particle. One lenticular pore forming. Location (15,1)

b. Many fingers, some detached from particles. Lenticular pores forming and moving into original particles. Location (13,2)

Figure 6. Finger Formation and Growth and Lenticular Pore Formation in DC-1

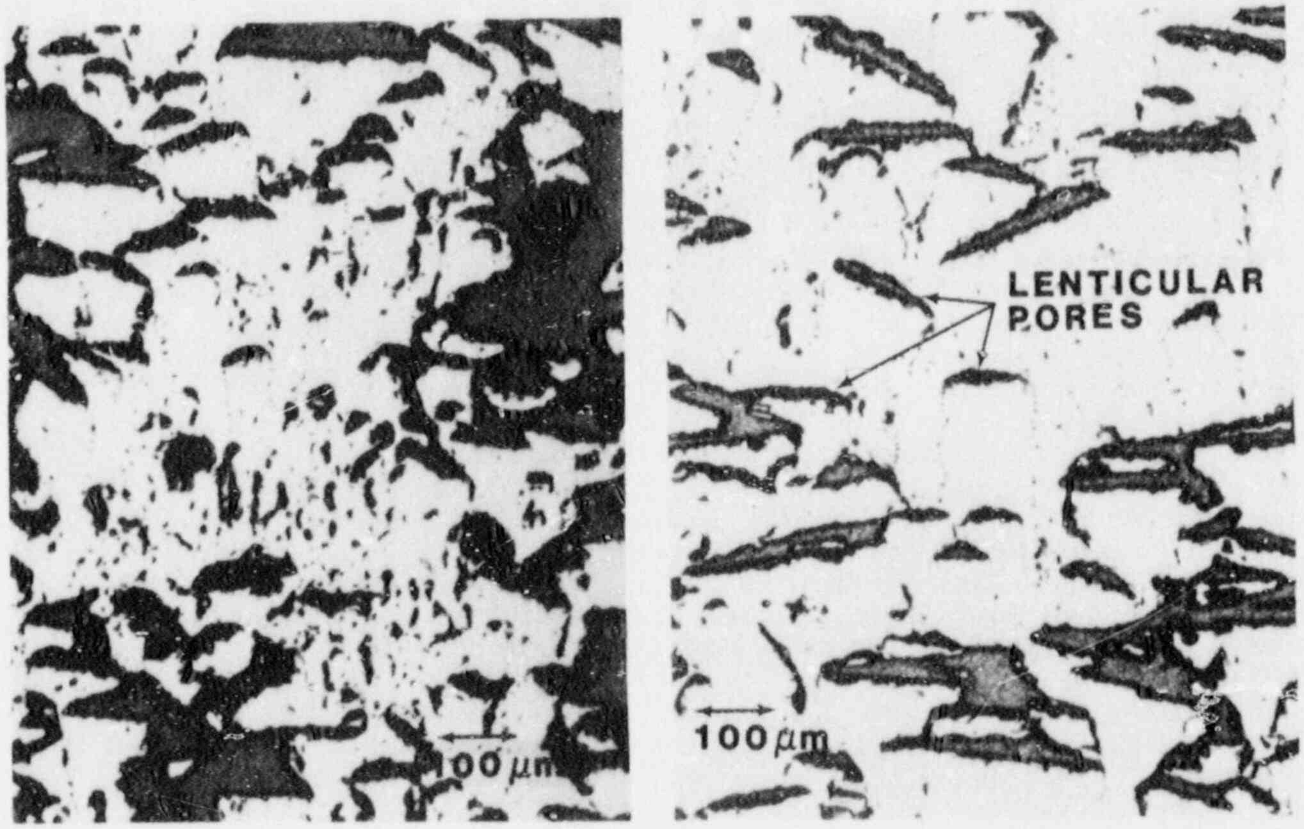


a. Many densified fingers growing towards lenticular pores moving towards the thermal center. Location (17,3)

b. Lenticular pores moving through restructured material. Location (20,5)

Figure 7. Lenticular Pores in DC-1

The molten zone, Zone 3, consists of a pool of once-molten material contained in the restructured material. The microstructure shows large, columnar grains typical of a material solidified in a temperature gradient. There is a small amount of microporosity; the pores, < 10 $\mu m$ in diameter, are distributed rather evenly between the grain boundaries and the grain interiors (Figure 9a and 9b). The polarized light reveals the grain structure.

The nature of the interface between the molten and restructured material is of interest. However, because the original interface between molten and non-molten material has been obliterated by lenticular pore movement subsequent to freezing and the apparent interface moved ~2 mm inward from the position of the original interface, it is not possible to know what the interface and pool region looked like immediately prior to $UO_2$ melting. Two hypotheses are presented. One is that a central void had formed due to lenticular pore movement and that the molten zone extended into a region of densified material containing numerous lenticular pores and fine porosity, but no linked porosity. This, with the good thermal mixing expected in the pool, would give rise to a very shallow interfacial region in which the distinction between molten and never-molten material would be quite clear. The second is that, at the time of the melt step, the bed was very porous and although lenticular pores had formed, there was little apparent densification of the bed because of its low initial packing density. (The bed would resemble Zone 3 of DC-2.) Then, upon melting, capillarity would pull the molten fuel out into the pores between particles. Such a structure was seen in a packed, $UO_2$ bed that was heated to incipient melting.[5]

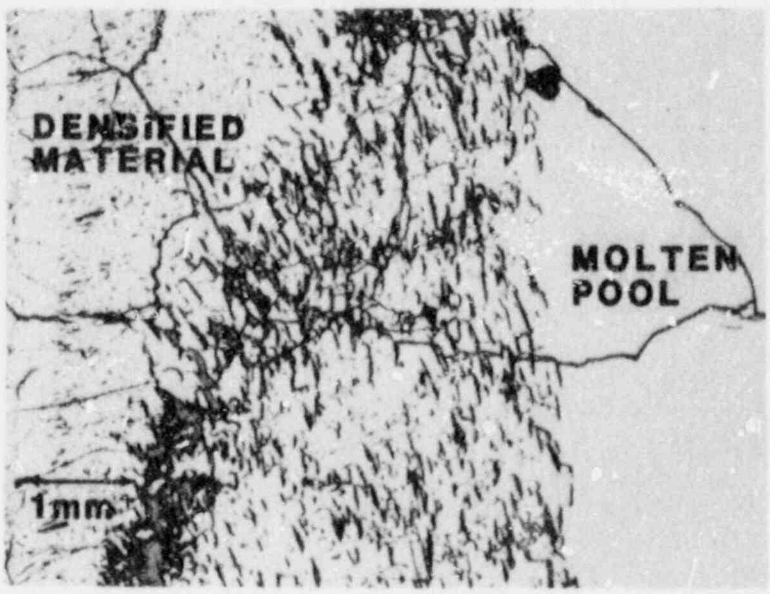


Figure 8. Material Densified by Lenticular Pore Migration in DC-1. There is no longer a vacancy source in the restructured material at the left. Location (2,25)

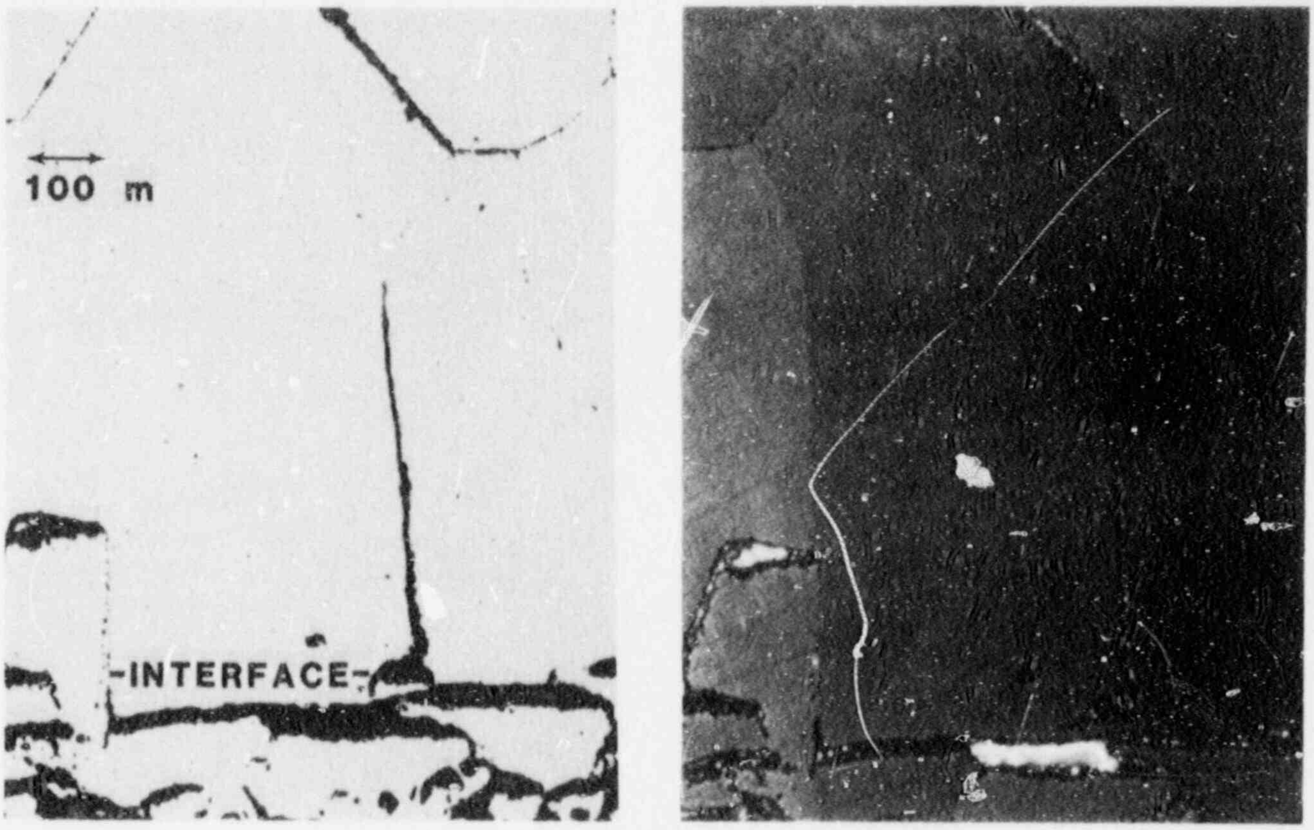


a. Location (20,10)

b. Same, polarized light

Figure 9. Interface Between Molten and Restructured Zones in DC-1

7.2 DC-2

DC-2 was heated in-pile to peak measured temperatures of ~2600°C. The average temperature gradient at peak power across the center of the bed was ~150°C/cm. The posttest appearance of the bed showed little macroscopic change in the $UO_2$ morphology (Figure 10). The steel was not distributed evenly over the bed. There was a central depleted region in a disc-shaped area ~2 cm high and 5 cm in diameter. This area was situated slightly above the midplane of the bed. Elsewhere, the steel had undergone local agglomeration to form irregular globules 1 to 5 mm in diameter and smaller spherical particles < 1 mm in diameter. These were distributed fairly evenly over the rest of the bed.

The description of the microstructure of DC-2 can be facilitated by considering three layers or shells. These are (1) the outer layer in which the steel is molten but little change is seen in the $UO_2$ (the steel melt zone), (2) the intermediate layer in which $UO_2$ transport and steel exodus begin (the $UO_2$ vapor transport zone), and (3) the inner layer in which lenticular pore migration and steel depletion are found (the lenticular pore migration zone) (Figure 11). The restructuring process is similar to that seen in DC-1 but is complicated by the presence of steel. Figure 12 shows a vertical strip through the center of the bed; Figure 13 shows a horizontal strip from the edge towards the center in the hot plane. The positions of these strips are shown in Figure 2b.

In the outer layer, Zone 1, where temperatures remained below ~2100°C, there was no significant change in the $UO_2$ particles as compared to the starting material. Steel particles fall roughly into two groups. There are large globules, 1 to 5 mm in diameter, with $UO_2$ particles adhered to their surfaces or, more rarely, embedded completely. This zone is shown in the left-most third of Figure 13, where the large (light-colored) steel globules are surrounded by the generally smaller, porous $UO_2$ particles. Generally, less than half of a $UO_2$ particle was enveloped in steel (Figure 14). The steel-$UO_2$ contact angle is $90° \pm 10°$. Standard usage in physics defines a contact angle of 0° (a sphere on a plane) as the occurrence of absolutely no wetting, 90° as the beginning of wetting, and 180° as perfect wetting. Here, there is only limited wetting. The small particles, 10 to 50 $\mu m$ in diameter, are spherical or hemispherical. This is recondensed material and is found on the $UO_2$ surfaces, where the same contact angle (90°) is seen. All of the steel in the outer layer had been molten.

In the intermediate layer, Zone 2, the first evidence of significant material transport was seen. Fingers of densified $UO_2$ formed on the up-gradient side of $UO_2$ particles. There is less steel here, especially, fewer of the large globules. There are large voids around which the $UO_2$ is distributed as it is around large steel globules in the outer areas; these seem to have once held steel. Zone 2 is seen in the right two-thirds of Figure 13 and the top and bottom fifths of Figure 12, where empty (dark) and half empty areas as well as light, steel globules are surrounded by $UO_2$ particles, the size of which is much smaller than those in Zone 1. A third steel morphology appeared in addition to the large and small particles: the $UO_2$ fingers contained layers of steel (Figure 15).

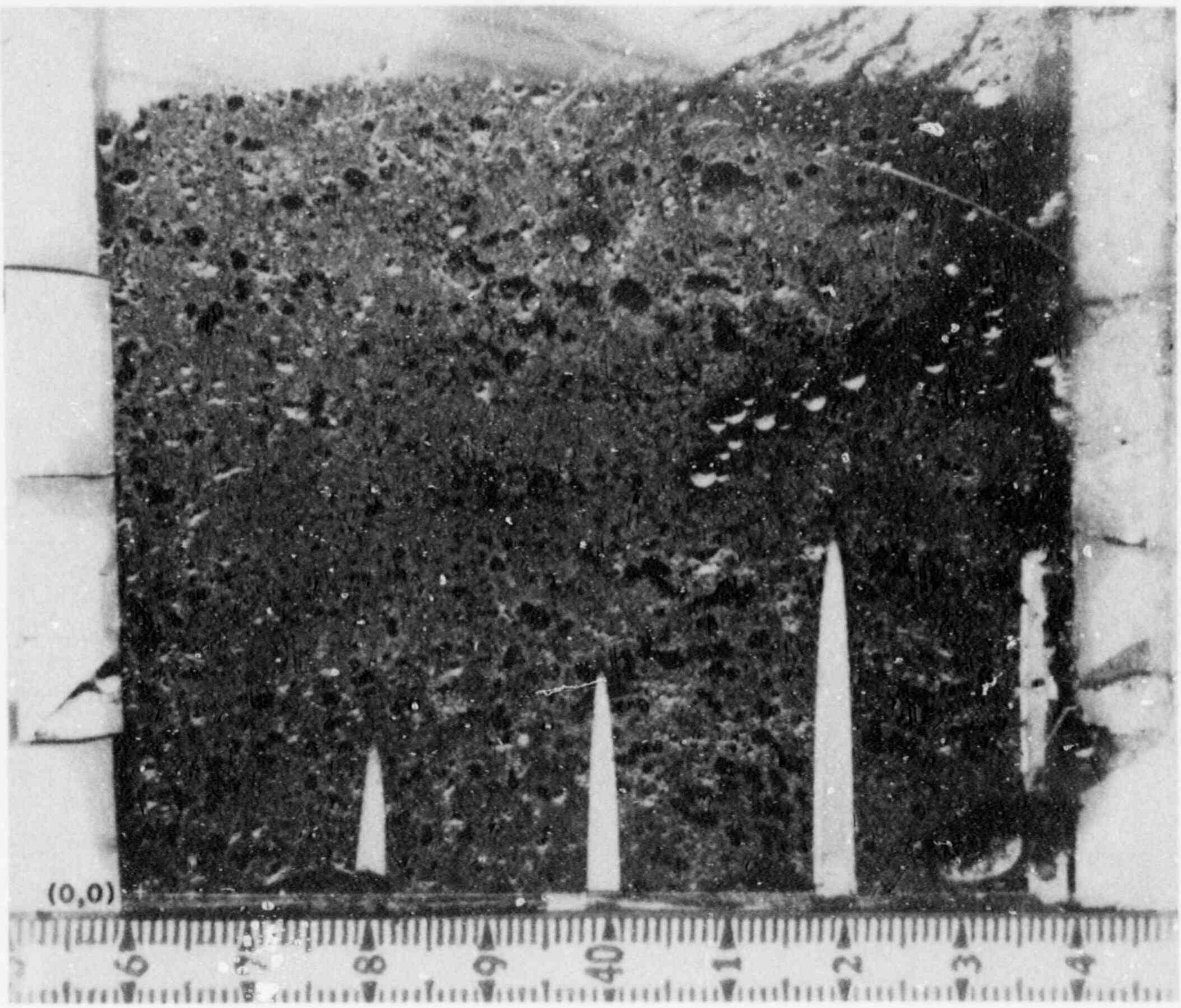


Figure 10. DC-2 Center Plane.
The location of subsequent micrographs is given in mm from the origin as shown.

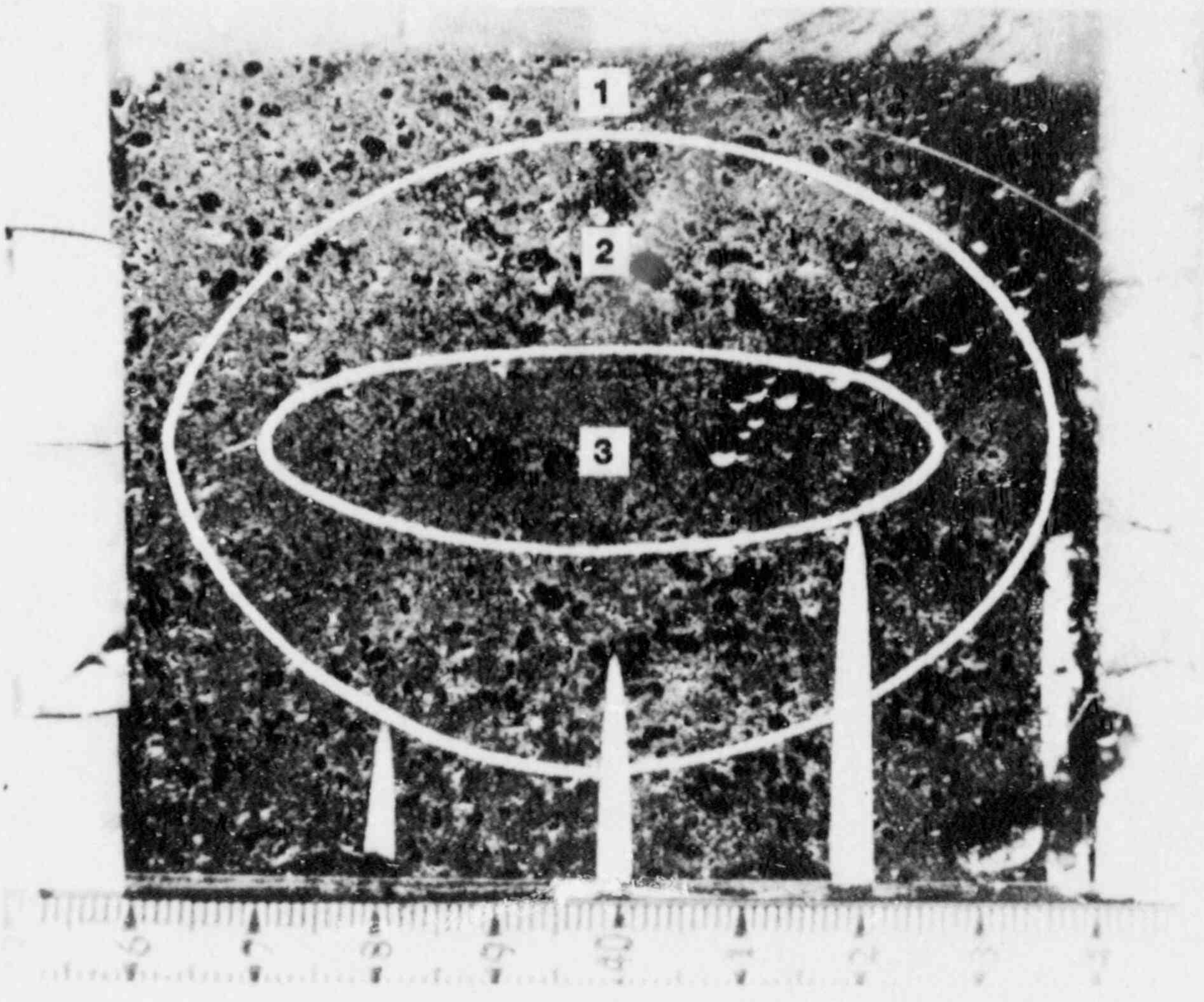


Figure 11. Steel Melt (1), $UO_2$ Vapor Transport (2), and Lenticular Pore Migration (3) Zones of DC-2

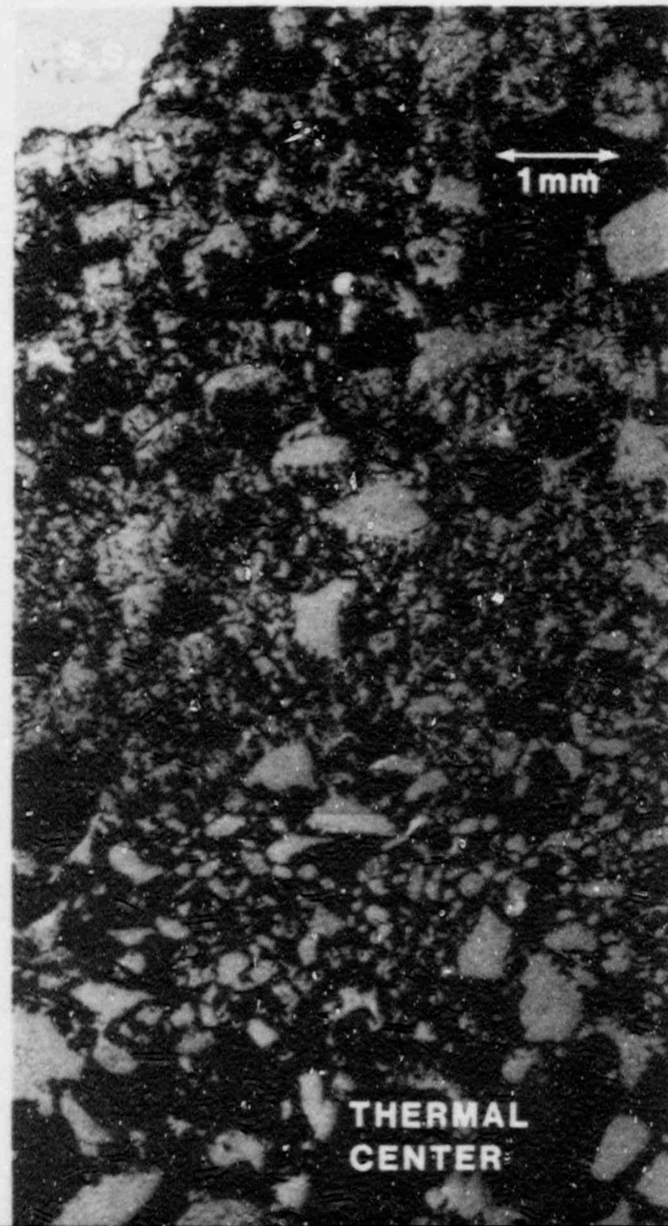
1mm
THERMAL
CENTER

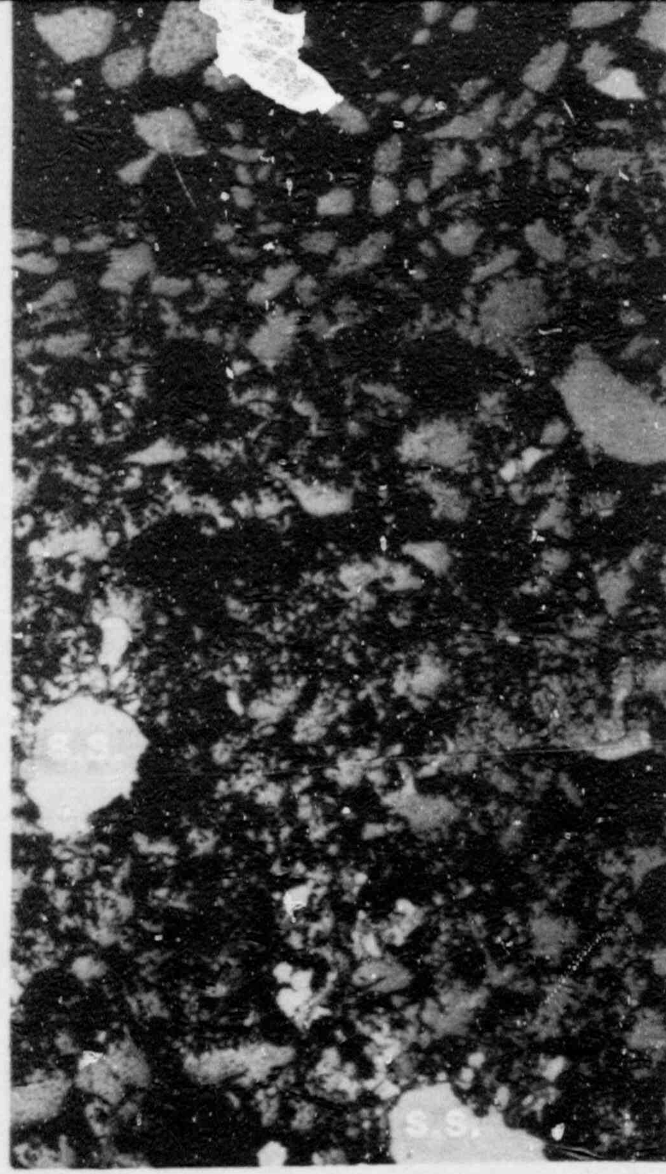


Figure 12. Vertical Strip Through Center of DC-2 Bed. Location at center of micrograph: (38,34).

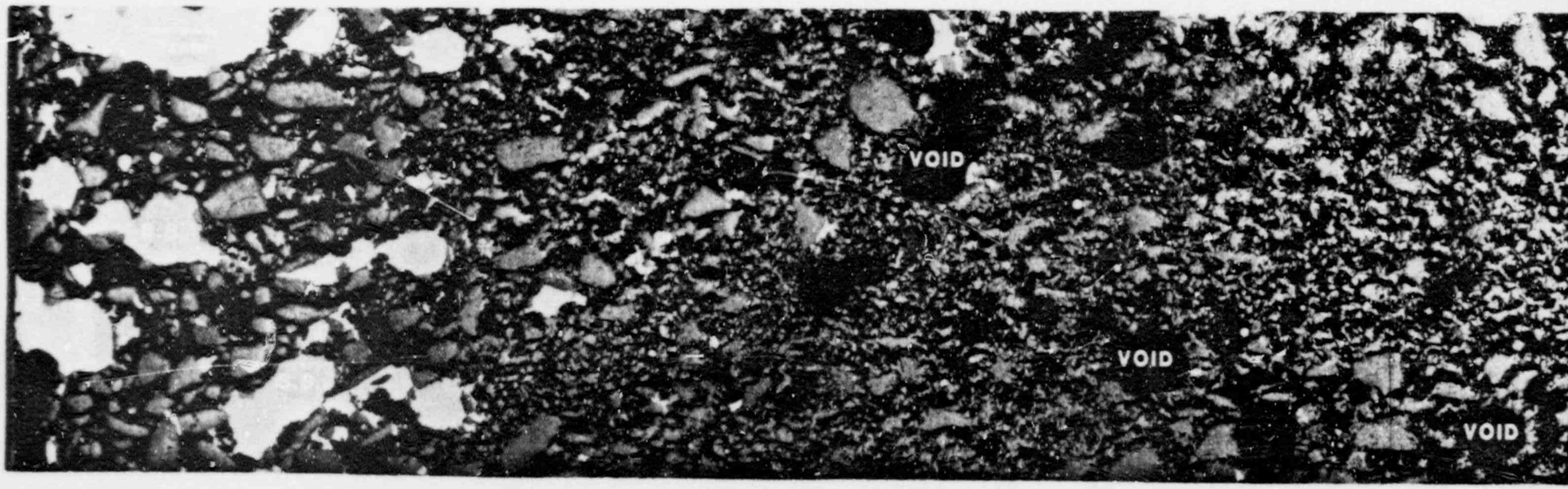


Figure 13. Horizontal Strip From Edge Towards Center of DC-2 Bed. Location at left edge of micrograph: (0,34).

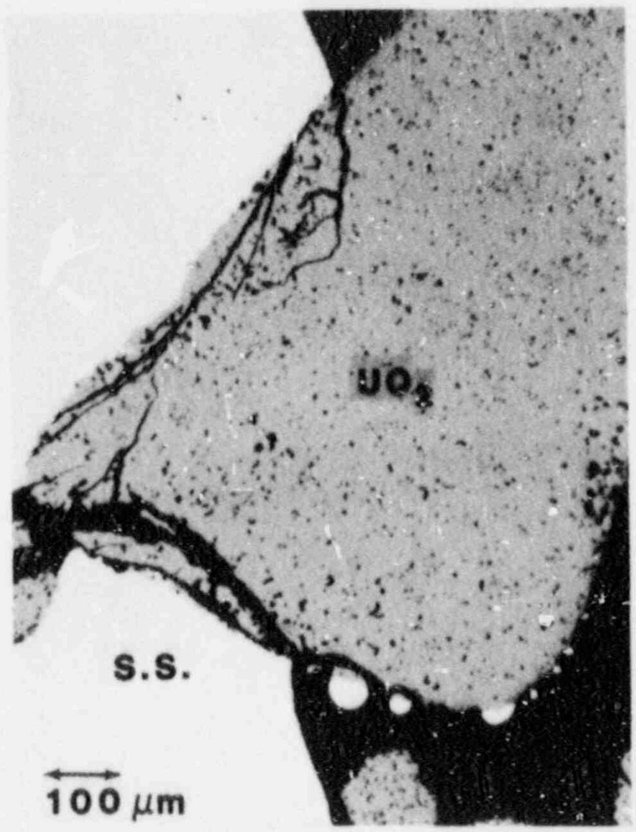


Figure 14. $UO_2$ Particle Partially Embedded in Steel Globule.
Location (64,70).

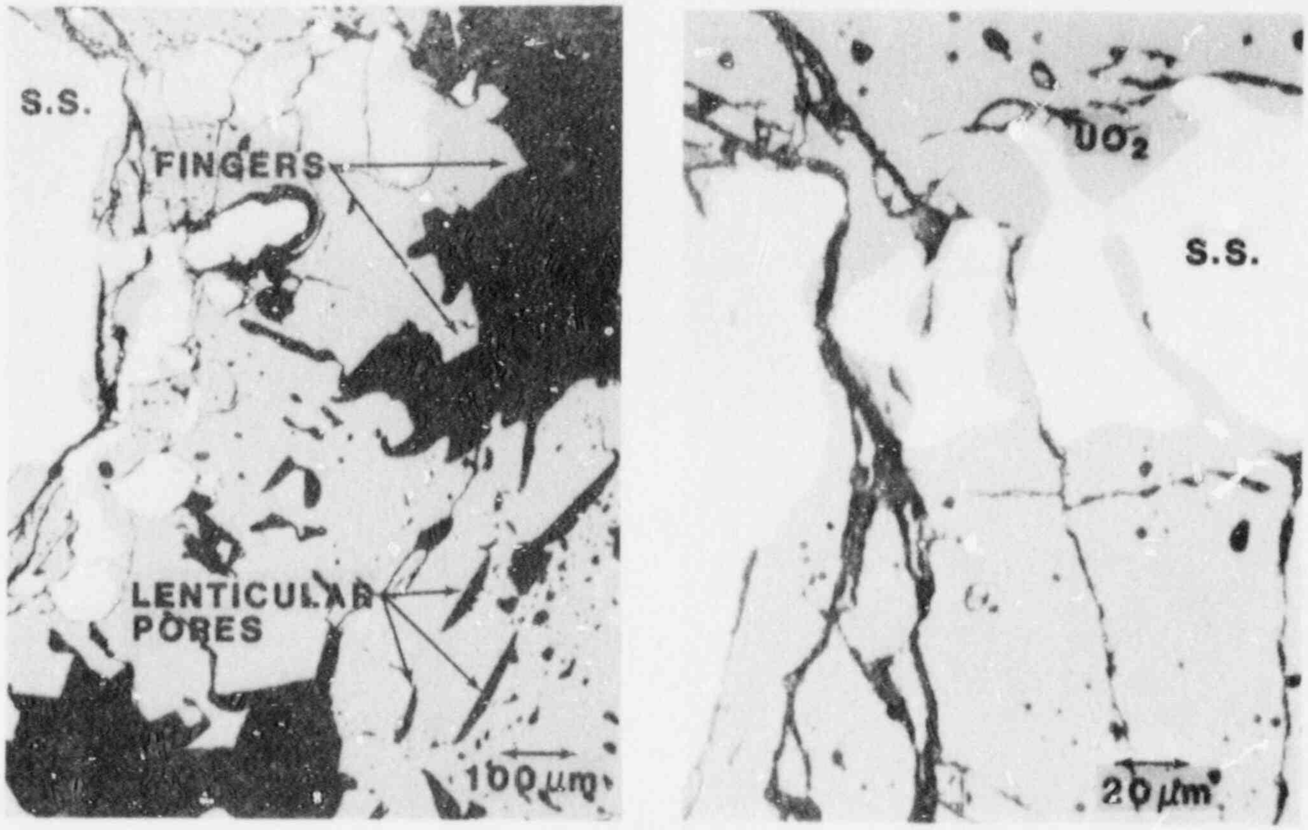


a. Vapor transported $UO_2$ and steel continguous with large steel globule. Location (20,42).

b. Layer structure steel and $UO_2$ fingers. Same area at higher magnification.

Figure 15. Steel Involvement in $UO_2$ Vapor Transport

The inner region, Zone 3, is characterized by lenticular pore formation and densification of the $UO_2$ by lenticular pore migration (Figure 16). Steel exodus from the large globules was common here. Small metal particles entirely enclosed by $UO_2$ are also visible. Steel depletion is extensive in a very thin disc within this inner region. Zone 3 is illustrated by Figure 13: large voids, very little steel, and lenticular pores in the fuel are seen.

Generally, the original appearance of the $UO_2$ particles has been lost in Zone 3. Very near the center of the bed there are, however, $UO_2$ particles that seem unchanged and lack densified fingers (Figure 17a) as well as small agglomerations of particles in which conventional sintering processes occurred (Figure 17b). These areas are encircled by densified fingers the orientation of which indicates that such areas were located at the thermal center--where there is no gradient--sometime during the experiment.

Steel behavior in the packed $UO_2$ bed heated in-pile was very different from behavior observed in earlier in- and out-of-pile experiments.[5,6,7,8] As the temperature of an area rose above the 316L stainless steel liquidus temperature, steel in that area began to melt. Coalescence of neighboring particles occurred, forming globules with a high surface tension. Loose $UO_2$ particles were pushed to the surface of the liquid metal. This small-scale coalescence of steel--as opposed to the large agglomerations seen with conventional heating--can be explained by the steep temperature gradient. The molten steel available in the area at a given time is limited: steel in the adjacent, hotter region has already undergone coalescence while steel in the adjacent cooler region is not molten. Hence, steel moving into the hot zone (by, for example, gravity or capillary action) does not encounter more steel immediately, and steel moving into the cold zone freezes. A globule apparently attains a stable configuration before there is an important local temperature rise. Two important differences between this and earlier tests, which could also account for the different steel behavior, are the initial oxygen content and steel morphology. In the earlier tests, water fragmented steel, which contained a large amount of oxygen and was in the form of 80- to 120-$\mu$m flakes was used.

In areas heated above ~2100°C, chromium depletion of the steel is seen. In Zone 2, in areas heated above ~2300 to 2400°C, steel evaporated from the globules and moved into the colder zone where it condensed. (Kim[9] found that the vapor pressure of 316L stainless steel became non-negligible above 2100°C and reached ~0.25 atm at 2500°C. He also found that the evaporation rate of 316 stainless steel reached 1 $g/cm^2 \cdot s$.) Entire globules of steel were removed from the hottest zone leaving empty shells of $UO_2$. Partially evaporated globules, with some steel remaining on the up-gradient (hot) end, are seen in the adjacent cooler region. The metal vapor condensed simultaneously with the $UO_2$ vapor on the up-gradient (hot) end of $UO_2$ particles. The condensed liquids apparently segregated quickly. The final morphology was a layered structure in which $UO_2$ and steel are distinct (Figure 15).


Figure 16. Lenticular Pore Formation and Movement Near the Center of the DC-2 Bed. Location (42,40).

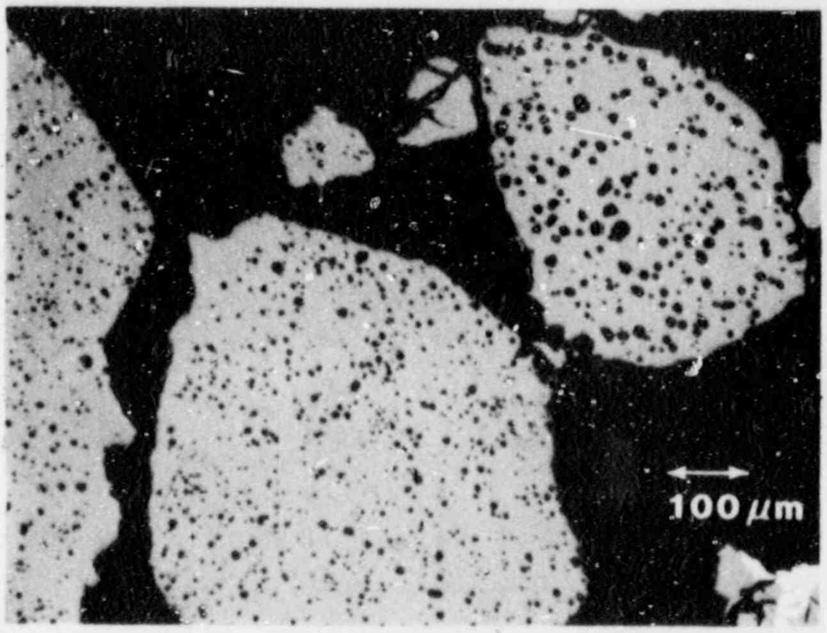


a. Apparently Unaffected $UO_2$ Particles in the Center of the DC-2 Bed.
Location (34,34).

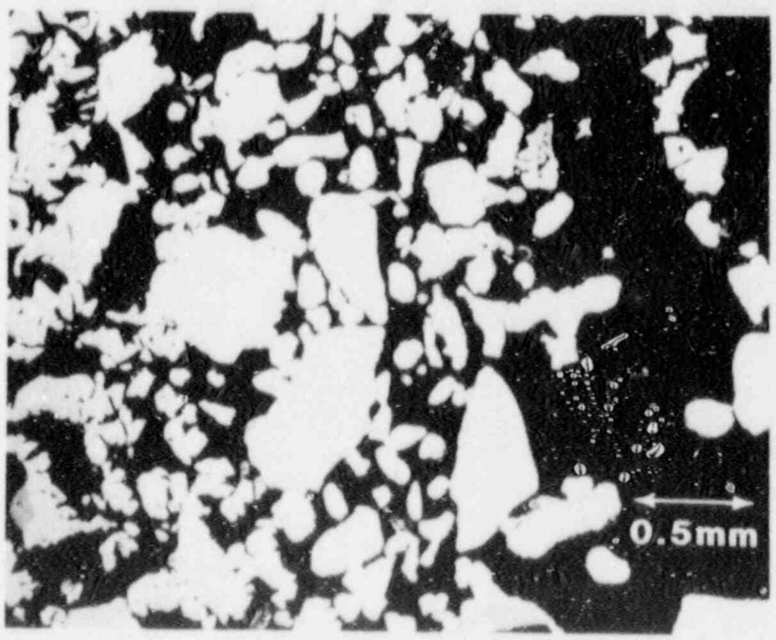


b. $UO_2$ Particles Joined by Conventional Sintering Processes. Note orientation of surrounding fingers and pores.
Location (25,35).

Figure 17. Areas Illustrating Behavior at Thermal Centers

Optically, the steel in the two outer layers appears to be a single phase. In the center are some multiple phase metallic particles with at least three phases (Figure 18). Nowhere is a boundary phase between $UO_2$ and steel seen.

Energy dispersive X-ray analyses of the metallic material in DC-2 were made at about 50 points in the bed from the left edge to the thermal center at 35 to 40 mm above the bottom of the bed. Elements lighter than sodium, such as oxygen, cannot be detected by this method. The results have been estimated to have a margin of error of < 10 percent. The results are displayed graphically in Figure 19. In the outer part of the bed, where large agglomerations of metal were seen, the metal was one phase, essentially stainless steel. Moving from 0 to 15 mm, the proportions of Cr, Mn, and Si were decreased while Fe, Ni, and Mo were concentrated. The Cr dropped from 20 wt% at the outer edge, which represents a gain of 3 percent from the as- fabricated composition, to 10 wt%; the Fe increased from 69 to 74 wt%, and the Ni from 9 wt%, a loss of 2 percent from the as-fabricated composition, to 14 wt%. There were no compositional gradients in contiguous material (i.e., agglomerations and fingers).

From 15 to 38 mm, the metal particles are much smaller and have a segregated or multiphase structure. There is no clear trend in compositional variation but these recurrent phases can be found: an Fe-rich phase with ~65 to 75 wt% Fe, balance (Cr, Ni, and Mo); a Mo-rich phase with ~40 to 50 wt% Mo, ~40 to 50 wt% Fe, and 10 wt% (Cr and Ni); and a U-rich phase of variable composition containing U with Fe, Ni, Cr, and Mo. The Mo-rich phase is first seen as the small droplets remaining in the $UO_2$ shells that once held steel. This phase is seen with the Fe-rich phase when the Mo solubility limit in "stainless steel" was exceeded due to the loss of the lower melting point components (Fe, Cr, and Ni) by vapor transport. The U-rich phase is seen only very near the center. Otherwise, no U is seen with the metallic material.

Analyses of large agglomerations of metal seen at ~8 mm above and below the hot center were also made. These were found to be essentially stainless steel (75 percent Fe, 15 percent Ni, and 10 percent Cr) depleted of Mo, Mn, and Si. There was a small amount of a second phase segregated in the grain boundaries.

The composition of $UO_2$ particles was analyzed at eight points from the edge to the center of the bed. No variation in composition was seen. Small amounts (< 1 wt%) of Fe and Cr were detected; these may be background from the microscope. No stoichiometry determination was performed.

## 8. SUMMARY AND CONCLUSIONS

The DC-1 and DC-2 experiments were sectioned and analyzed. In DC-1, a pure $UO_2$ bed, measured peak temperatures ranged from 3100°C in the center of the bed to 2500°C at the edge. The posttest configuration consisted of a shell of restructured fuel holding a once-molten pool of $UO_2$ with a large overlying void. The grain structure at the pool surface indicated that the heat removal from the top was nearly equal to that of the side. Outside of the shell was an unaffected region composed of $UO_2$ particulate occupying the very top and bottom of the bed. The mass of the once-molten pool was approximately 1.2 kg, over half of the original debris mass. The large void above the pool comprised 25 to 30 vol% of the total configuration and was primarily due to the difference in porosity between the initial bed and the molten pool. The initial open porosity in the bed was 40 percent, which allowed some compaction during the experiment; the final void volume above the pool accounted for a large fraction of the total original porosity in the bed, indicating that porosity is "captured" during the crust formation.

The densification and agglomeration of $UO_2$ in forming the crust at elevated temperatures and in the presence of a steep thermal gradient did not proceed by conventional sintering processes. The process noted in DC-1 was dominated by $UO_2$ vapor transport and, although supporting evidence was obliterated, probable densification due to capillary action during molten pool formation. Temperatures exceeding ~2000 to 2100°C were sufficent to initiate vapor transport. The $UO_2$ was transported to cooler regions where it condensed. This resulted in an initial decrease in particle size in the center and a densification in the outer zones. This is evidenced by the formation of high density fingers on particles in the outer regions. The fingers grew and some contacted other particles to form lenticular pores. As the $UO_2$ transport proceeded, the characteristic starting particulate debris with open porosity was transformed into a dense material with closed lenticular porosity. Vapor transport, driven by the thermal gradient, was then restricted to within the pore itself. The net effect is that the lenticular pores migrated up the thermal gradient through previously densified fuel until they reached a free surface. The interface between the molten $UO_2$ and the crust during the heating phase had been obliterated by pore movement subsequent to freezing. This mechanism of densification due to $UO_2$ vapor transport, probably combined with capillarity during melting, led to coherent high density crusts capable of supporting overlying melts.


a. Location (36,34)


b. Same as a


c. Location (40,36)


d. Same as c

Figure 18. Two Multiphase Metallic Particles in the Center of the DC-2 Bed

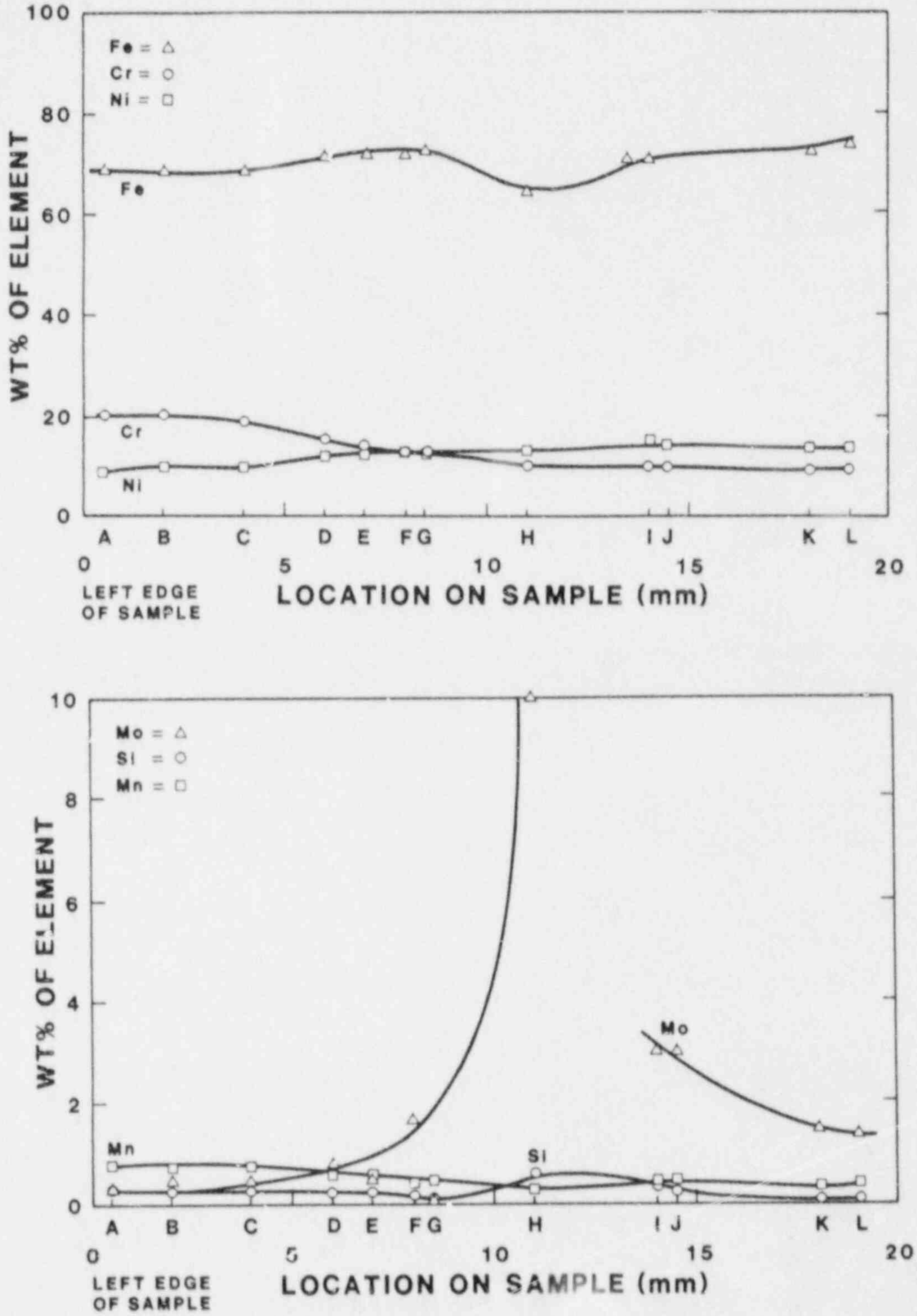


Figure 19. Composition as a Function of Radial Position in the DC-2 Bed

The apparent sequence for formation of the molten pool involved initial loss of material from the central region, densification of outer regions, melting and pool formation in the center, expansion of the crust, and enlargement of the molten pool and overlying void. Because of the extensive restructuring, there was no evidence of initial material motion being driven by capillary force. With sustained heating in a large bed, the crust moved outward until encountering temperatures at which the $UO_2$ vapor pressure was insufficient to allow significant material motion. The integrity of the crust above the void is important in the event of a quench or reflood in order to prevent large amounts of coolant from interacting with the molten pool. In the experiment, the 3100°C molten pool was stabilized within the crust, which acted as a containment, given the cooled boundaries.

The DC-2 experiment, which included 25 wt% stainless steel debris, was limited to a peak measured temperature of 2600°C in order to avoid $UO_2$ melt and hence to emphasize the effects of steel melt and migration. All of the steel in the bed was molten. The structure of DC-2 is best described by three regions or shells. The inner region or central zone (highest temperature) is largely devoid of steel, and the $UO_2$ particulate has lost some material by the vapor transport mechanism identified in DC-1. Toward the edge of thi region there is evidence of $UO_2$ densification, finger formation, and some lenticular pore formation. There are fairly round void areas surrounded by $UO_2$, which appear to have once held steel agglomerated earlier in the experiment at lower temperatures. The intermediate region shows clear evidence of $UO_2$ transport by the presence of densified $UO_2$ fingers. Some of the fingers contain layers of steel. Spherical void areas are also present and some still contain steel remnants. In the outer area there is essentially no change in the $UO_2$ particle morphology. The steel morphology falls roughly into two types: large globules, 1 to 5 mm in diameter, whose shape is defined by the adjacent $UO_2$ particulate and small particles, 10 to 50 $\mu$m in diameter, which are spherical in shape. The steel-$UO_2$ contact angle is $90° \pm 10°$.

Elemental analysis of the steel in the bed indicates that steel in the outer region is single phase and essentially "stainless steel" in composition. In the intermediate zone, there are indications that the lower volatility constituents of the steel were lost, while there was concentration of the Mo. There are also multiphase structures with a Mo-rich phase. The Mo-rich phase is also seen as remnants in the $UO_2$ shells, which once contained large globules of stainless steel. No boundary phase and no alloying is evident between the molten steel and the $UO_2$. The steel behavior in the experiment is described by the following: Above the steel liquidus temperature, the steel melts and coalesces with neighboring particles to form globules. The high surface tension tends to displace the $UO_2$ particulate to the surface of the melt. At temperatures above -2300° to 2400°C, the steel evaporates from the globules and condenses in the cooler outer regions. Hence the steel transport mechanism is similar to the $UO_2$ transport in DC-1 in that it is dominated by vapor effects.

The behavior of the steel in DC-2 was markedly different from previous furnace and in-pile tests where the steel migrated and agglomerated into large masses randomly without any preferred location or direction. The interaction of the steel with the $UO_2$ and movement of the steel is important to understand since it influences development of molten pools and affects the heat transfer in the bed. The results here indicate that at elevated temperatures with large temperature gradients, the steel will accumulate in the cooler outer regions. The surface tension of the steel tends to hold it in place in the $UO_2$ matrix where it condenses rather than relocating to the bottom by gravity. Hence, with large beds where the steel may condense and freeze at the boundaries, a layer is formed of a steel-rich material that would remelt at much lower temperatures than $UO_2$ melt. Even with the steel relocation, the thermal conductivity of the bed increased significantly. The initial conclusion derived from the thermal data was that the steel migration, if any, was toward the center of the bed since the central temperatures were depressed. This is consistent with the earlier tests. However, it is clear in DC-2 that the central region was largely devoid of steel. Contributing reasons for the increased average thermal conductivity of the bed are that the steel path length has increased up to a factor of 10, there is intimate contact between the steel and urania, and there is interconnection of the urania. The zone depleted of steel in the center is a fairly small fraction of the bed. Moreover, the $UO_2$ migration from the central area moves the heat source to the outer regions.

It is postulated that if the bed power had been increased to produce $UO_2$ melt, the remaining steel in the central region would have been transported to the outer areas and the molten pool, composed largely of $UO_2$, would have been similar to that of DC-1. A multilayered crust with an outer layer of stainless steel and $UO_2$ particulate, an intermediate mixed layer, and an inner layer of densified $UO_2$ would be expected.

In conclusion, the two experiments have identified the important governing phenomena associated with the transition from a debris bed to a molten pool configuration. At elevated temperatures in the presence of large thermal gradients, material motion of both stainless steel and urania is dominated by vapor transport.

## 9. REFERENCES


1. J. T. Hitchcock and J. E. Kelly, The DC-1 and DC-2 Debris Coolability and Melt Dynamics Experiments, Sandia National Laboratories, Albuquerque, NM, NUREG/CR-4060, SAND84-1367, April 1985.

2. G. M. Fair and L. P. Hatch, "Fundamental Factors Governing Streamline Flow of Water through Sand," J. Amer. Water Works, 25, 1551-1565 (1933).

3. M. E. Field, Development of Ultrasonic Thermometry for High-Temperature High-Resolution Temperature Profiling Applications in LMFBR Safety Research, Sandia National Laboratories, Albuquerque, NM, SAND84-1341, May 1986.

4. D. R. Olander, Fundamental Aspects of Nuclear Reactor Fuel Elements, Technical Information Center, ERDA, Washington, TID-26711-P1, 1976, 133, 265-273.

5. J. T. Hitchcock and J. E. Kelly, "Post-Test Examinations of the In-Pile Molten Pool Experiments," Trans. ANS, 43, 515-6 (1982).

6. D. W. Varela, "Molten Steel Behavior in PAHR Debris Beds," Trans. ANS, 38, 388-9 (1981).

7. H. G. Plein and G. A. Carlson, "Debris Bed and Sacrificial Materials Interaction at High Temperatures," Trans. ANS, 30, 436, 1978.

8. S. F. Duliere and D. J. Sasmor, "Posttest Examination of Debris Bed -- Molten Pool Materials," Internal Memorandum, November 1983.

9. C. S. Kim, Thermophysical Properties of Stainless Steels, Argonne National Laboratories, Argonne, IL, ANL-75-55*, September, 1975.

DISTRIBUTION:

US Government Printing Office
Receiving Branch (Attn: NRC Stock)
8610 Cherry Lane
Laurel, MD 20707
(200 Copies for R7)

Div. of Reactor Safety Research (14)
Office of Nuclear Regulatory Research
US Nuclear Regulatory Commission
Washington, DC 20555
Attn: E. S. Beckjord
C. N. Kelber
T. L. King
R. O. Meyer
B. M. Morris
D. F. Ross
M. Silberberg
R. W. Wright (5)
G. P. Marino
P. M. Wood

Joint Research Center (10)
Ispra Establishment
21020 Ispra (Varese)
Italy
Attn: R. Klersy
K. Mehr
P. Fasoli-Stella
O. Simoni (5)
P. Schiller
H. Meister

Power Reactor & Nuclear Fuel
Development Corp. (PNC) (6)
Fast Breeder Reactor Development
Project (FBR)
9-13, 1-Come, Akasaka
Minato-Ku, Tokyo
Japan
Attn: A. Watanabe (2)
H. Nakamura
M. Saito
K. Takahashi
A. Furutani

Belgonucleaire
Rue du Champ de Mars 25
B-1050 Brussels, Belgium
Attn: J. Basselier

S.C.K./C.E.N.
Boeretang 200
B-2400 MOL
Belgium
Attn: C. J. M. Foly

Monsieur A. Schmitt
IPSN/DSN
CEN Fontenay-aux-Roses
B.P. 6
92260 Fontenay-aux-Roses
France

Safety Studies Laboratory/DSN (6)
Commissariat a L'Energie Atomique
Centre d'Etudes Nucleaires de Cadarache
B.P. 1, 13115 Saint-Paul-lez-Durance
Bouches-du-Rhone
France
Attn: M. Schwarz
M. Bailly
M. Meyer Heine
M. Penet
G. Kayser
C. LeRigoleur

Centre d'Etudes Nucleaires de Grenoble (2)
B. P. 85-Centre de Tri
38401 Grenoble Cedex
France
Attn: M. Costa/STT
D. Rousseau/Pi-SEDTI

UKAEA (2)
Safety and Reliability Directorate
Wigshaw Lane Culcheth
Warrington, WA3 4NE
United Kingdom
Attn: M. Hayns
R. S. Peckover

Atomic Energy Establishment (6)
Winfrith, Dorchester
United Kingdom
Attn: R. V. Macbeth
R. Potter
G. L. Shires
G. F. Stevens
R. Trenberth
T. Butland

Culham Laboratory (3)
Culham Abingdon
Oxfordshire OX14 3DB
United Kingdom
Attn: F. Briscoe
B. Turland
K. A. Moore

Kernforschungszentrum Karlsruhe (8)
D-75 Karlsruhe
Postfach 3640
West Germany
Attn: G. Heusener (PSB)
H. Werle (INR)
L. Barleon (IRB)
G. Hoffman (IRM)
K. Thomauske (IRB)
U. Muller (IRM)
G. Fieg (INR)
G. Schumacher (INR)

University of California (2)
Energy and Kinetics Department
Rm. 5405 Bolter Hall
Los Angeles, CA 90024
Attn: I. Catton
U. K. Dhir

Argonnne National Laboratory (5)
Reactor Analysis and Safety Division
9700 South Cass Avenue
Argonne, IL 60439
Attn: L. Baker, Jr.
J. C. Cassulo
J. D. Gabor
R. D. Pedersen
E. S. Sowa

General Electric Company
6835 Via del Ora
San Jose, CA 95119
Attn: E. Gluekler

Westinghouse Electric Corp. (2)
Power Systems
P.O. Box 355
Pittsburgh, PA 15230
Attn: L. Hockreiter
D. Squarer

Westinghouse Research and
  Development Center
Pittsburgh, PA 15235
Attn: A. Pieczynski

Nuclear Safety Analysis Center
3412 Hillview Avenue
P.O. Box 10412
Palo Alto, CA 94303
Attn: G. Thomas

Fauske and Associates (2)
631 Executive Dr.
Willowbrook, IL 60521
Attn: M. Epstein
      R. Henry

Brookhaven National Laboratories (2)
Fast Reactor Safety
Upton, Long Island, NY 11973
Attn: J. W. Yang
      T. Ginsberg

Los Alamos National Laboratories
Q7, Slot K556
Los Alamos, NM 87545
Attn: Javiei Escamilla

NUS Corporation
Consulting Division
4 Research Place
Rockville, MD 20850
Attn: Juan M. Nieto

EG&G Idaho (3)
P.O. Box 1625
Idaho Falls, ID 83415
Attn: C. Allison
      D. Croucher
      R. W. Miller

Mass. Inst. of Tech. (2)
Mechanical Engr. Dept.
Cambridge, MA 02139
Attn: P. Griffith
      M. Kazimi

University of New Mexico
Nuclear Engineering Department
Albuquerque, NM 87131
Attn: M. El-Genk

University of Wisconsin (2)
Department of Nuclear Engineering
Madison, WI 53706
Attn: M. L. Corradini
S. Abdel-Khalik

University of California
Chemical and Nuclear Eng. Dept.
Santa Barbara, CA 93106
Attn: T. Theofanous

| | |
|---|---|
| 6400 | D. J. McCloskey |
| 6410 | N. R. Ortiz |
| 6418 | J. E. Kelly |
| 6420 | J. V. Walker |
| 6421 | P. S. Pickard |
| 6422 | D. A. Powers |
| 6423 | K. O. Reil |
| 6425 | W. J. Camp |
| 6425 | A. W. Reed |
| 6427 | M. Berman |
| 6440 | D. A. Dahlgren |
| 6450 | T. R. Schmidt (5) |
| 6451 | T. F. Luera |
| 6452 | J. W. Bryson |
| 6454 | G. L. Cano |
| 6454 | C. P. Fryer (20) |
| 3141 | S. A. Landenberger (5) |
| 3151 | W. L. Garner |
| 8524 | P. W. Dean |

NRC FORM 335 (2-87)
NRCM 1102, 3201, 3202

U.S. NUCLEAR REGULATORY COMMISSION

# BIBLIOGRAPHIC DATA SHEET

SEE INSTRUCTIONS ON THE REVERSE

1. REPORT NUMBER (Assigned by PPMB, DPS, add Vol. No., if any)
NUREG/CR-4625
SAND86-1102

2. TITLE AND SUBTITLE
The Postirradiation Examination of the DC Melt Dynamics Experiments

3. LEAVE BLANK

4. DATE REPORT COMPLETED

| MONTH | YEAR |
|---|---|
| October | 1987 |

5. AUTHOR(S)
C.P. Fryer, J.T. Hitchcock

6. DATE REPORT ISSUED

| MONTH | YEAR |
|---|---|
| July | 1988 |

7. PERFORMING ORGANIZATION NAME AND MAILING ADDRESS (Include Zip Code)
Sandia National Laboratories
Albuquerque, NM 87185

8. PROJECT/TASK/WORK UNIT NUMBER

9. FIN OR GRANT NUMBER
FIN A1181

10. SPONSORING ORGANIZATION NAME AND MAILING ADDRESS (Include Zip Code)
Division of Reactor Accident Analysis
Office of Nuclear Regulatory Research
U.S. Nuclear Regulatory Commission
Washington, DC 20555

11a. TYPE OF REPORT
Technical

b. PERIOD COVERED (Inclusive dates)

12. SUPPLEMENTARY NOTES

13. ABSTRACT (200 words or less)

The results of the postirradiation examination of two dry debris beds composed of (1) pure $UO_2$ and (2) mixed $UO_2$ and stainless steel are presented. In the $UO_2$ bed, approximately 50% of the bed formed a molten pool which was surrounded by a high density crust. Lenticular pore formation and migration due to $UO_2$ vapor transport in the strong thermal gradient were seen in the crust. In the mixed $UO_2$ and steel bed, all of the steel had been molten. Steel and $UO_2$ migration were observed; both were thought to be caused by vapor transport mechanisms.

14. DOCUMENT ANALYSIS - a. KEYWORDS/DESCRIPTORS
postirradiation examination
debris bed
core debris
molten $UO_2$ pool
heat flux

b. IDENTIFIERS/OPEN-ENDED TERMS

15. AVAILABILITY STATEMENT
Unlimited

16. SECURITY CLASSIFICATION
(This page)
Unclassified
(This report)
Unclassified

17. NUMBER OF PAGES

18. PRICE

UNITED STATES
NUCLEAR REGULATORY COMMISSION
WASHINGTON, D.C. 20555

OFFICIAL BUSINESS
PENALTY FOR PRIVATE USE, $300

SPECIAL FOURTH CLASS RATE
POSTAGE & FEES PAID
USNRC
PERMIT No. G-67

120555078877 1 1AN1R7
US NRC-OARM-ADM
DIV OF PUB SVCS
POLICY & PUB MGT BR-PDR NUREG
P-210
WASHINGTON DC 20555

NUREG/CR-4625 POSTIRRADIATION EXAMINATION OF THE DC MELT DYNAMICS EXPERIMENTS JULY 1988